Eur. Phys. J. C 42, 281–301 (2005)
Digital Object Identifier (DOI) 10.1140/epjc/s2005-02298-5

THE EUROPEAN PHYSICAL JOURNAL C

Vector-meson electroproduction at small Bjorken-x and generalized parton distributions

S.V. Goloskokov[1,a], P. Kroll[2,b]

[1] Bogoliubov Laboratory of Theoretical Physics, Joint Institute for Nuclear Research, Dubna 141980, Moscow region, Russia
[2] Fachbereich Physik, Universität Wuppertal, 42097 Wuppertal, Germany

Received: 3 February 2005 / Revised version: 9 May 2005 /
Published online: 28 June 2005 –

Abstract. We analyze electroproduction of light vector mesons ($V = \rho, \phi$) at small Bjorken-x in an approach that includes the gluonic generalized parton distributions and a partonic subprocess, $\gamma g \to (q\bar{q})g$, $q\bar{q} \to V$. The subprocess is calculated to lowest order of perturbative QCD taking into account the transverse momenta of the quark and antiquark as well as Sudakov suppressions. Our approach allows us to investigate the transition amplitudes for all kinds of polarized virtual photons and polarized vector mesons. Modeling the generalized parton distributions through double distributions and using simple Gaussian wavefunctions for the vector mesons, we compute the longitudinal and transverse cross sections at large photon virtualities as well as the spin-density matrix elements for the vector mesons. Our results are in fair agreement with the findings of recent experiments performed at HERA.

1 Introduction

Vector-meson electroproduction at large photon virtuality, Q^2, has always attracted a lot of theoretical interest. Its diffractive nature as well as the interesting correlation between the Q^2 and the energy dependence are challenging issues. At first traditional concepts like vector-meson dominance (see e.g. [1]) or the Regge model with its prominent pomeron exchange (see e.g. [2]) have been exploited to analyze the electroproduction data. In 1987 Donnachie and Landshoff [3] viewed the pomeron as the exchange of two gluons between the proton and the quark–antiquark pair created by the virtual photon and which subsequently form the outgoing meson. Brodsky et al. [4] treated the two-gluon exchange contribution to electroproduction at large Q^2 and small Bjorken-x, $x_{\rm Bj}$, in the framework of QCD factorization. They showed that in their approach, known as the $\ln(1/x_{\rm Bj})$ approximation, the emission and reabsorption of the gluons by the proton can be related to the usual gluon distribution. Many variants of the leading $\ln(1/x_{\rm Bj})$ approximation can be found in the literature which differ mainly by the treatment of the subprocess $\gamma^* g \to Vg$; see [5–8] to name a few. These approaches describe many features of vector-meson electroproduction quite well.

In 1996 vector-meson electroproduction has been taken up by theory again. Exploiting the new concept of generalized parton distributions (GPD) [9,10] it has been shown [9,11] that, at large Q^2, the process factorizes into a hard parton-level subprocess – meson electroproduction off partons – and soft proton matrix elements which represent generalized parton distributions. The process is depicted in Fig. 1 where also the momenta of the involved particles are specified. It has also been shown in [9,11] that the process is dominated by transitions from longitudinally polarized photons to longitudinally polarized vector mesons ($\mathrm{L} \to \mathrm{L}$) at large Q^2; the amplitudes for other transitions are suppressed by inverse powers of Q. The production of vector mesons at small $x_{\rm Bj}$ ($\lesssim 10^{-2}$) is controlled by gluonic GPDs where quasi-on-shell gluons are emitted and reabsorbed by the proton. These GPDs which represent the soft physics embodied in the proton matrix elements, are unknown as yet and have to be modelled.

Detailed experimental information on electroproduction of light vector mesons in the region of small $x_{\rm Bj}$ is available from HERA. Cross sections and spin-density matrix elements have been measured by H1 [12] and ZEUS [13,14]. Despite the sound theoretical basis of the handbag approach not much has been done as yet in analyzing these data within this framework. There is only the explorative study of the longitudinal cross section for ρ production performed by Mankiewicz et al. [15]. The normalization of the cross section was however not understood in this work. Martin et al. [8], on the other hand, started from the $\ln(1/x_{\rm Bj})$ approximation and estimated effects due to the replacement of the gluon distribution by the corresponding GPD. Here, in this work we attempt a complete and systematic analysis of the available electroproduction data at small $x_{\rm Bj}$. In order to analyze the spin-density matrix elements of the vector mesons we also calculate the ampli-

[a] e-mail: goloskkv@thsun1.jinr.ru
[b] e-mail: kroll@physik.uni-wuppertal.de

tudes for transitions from transversely polarized photons to transversely and longitudinally polarized vector mesons ($T \to T$ and $T \to L$). We allow for quark transverse momentum and take into account Sudakov suppressions. As it will turn out, this approach leads to the correct normalization of the cross sections at finite but large Q^2. Infrared singularities which occur for the $T \to T$ transition amplitude in collinear approximation [16], are also regularized in our approach although in an admittedly model-dependent way.

The plan of this paper is the following: A kinematical prelude and the handbag amplitude are presented in Sect. 2. The amplitudes for the subprocess $\gamma^* g \to V g$ are discussed in Sect. 3 to leading order of perturbative QCD and including transverse momenta of the quarks and antiquarks making up the meson. The impact parameter representations of the full handbag amplitudes for electroproduction of vector mesons are presented in Sect. 4. The following section, Sect. 5, is devoted to the construction of the GPDs. Numerical results, obtained from the handbag approach, for the cross sections of vector-meson electroproduction and for the vector meson's spin-density matrix elements are compared to recent experimental results in the small $x_{\rm Bj}$ region in Sects. 6 and 7, respectively. In the next section, Sect. 8, we discuss the helicity correlation $A_{\rm LL}$ and the role of the GPD $\widetilde{H}$ and summarize in Sect. 9.

2 The handbag factorization

We will work in a photon–proton center of mass (CM) frame, see Fig. 1, in a kinematical situation where

$$W^2 \,=\, (p+q)^2\,, \tag{1}$$

and the virtuality of the incoming photon, $q^2 = -Q^2$, are large while Bjorken's variable,

$$x_{\rm Bj} \,=\, Q^2/(2p\cdot q)\,, \tag{2}$$

is small ($x_{\rm Bj} \lesssim 10^{-2}$). We also assume the square of the momentum transfer, $\Delta = p' - p$, to be much smaller than Q^2.

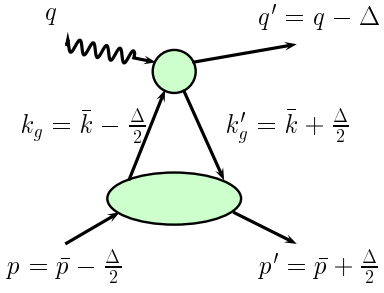

Fig. 1. The handbag-type diagram for meson electroproduction off protons. The large blob represents a GPD while the small one stands for meson electroproduction off partons. The momenta of the involved particles are specified

In light-cone components, defined by $a^\pm = (a^0 \pm a^3)/\sqrt{2}$ and $a\cdot b = a^+b^- + a^-b^+ - \mathbf{a}_\perp \mathbf{b}_\perp$, the momenta of the protons and the photon read

$$\begin{aligned} p &= \left[(1+\xi)\bar{p}^+, \frac{m^2+\mathbf{\Delta}_\perp^2/4}{2(1+\xi)\bar{p}^+}, -\frac{\mathbf{\Delta}_\perp}{2}\right], \\ p' &= \left[(1-\xi)\bar{p}^+, \frac{m^2+\mathbf{\Delta}_\perp^2/4}{2(1-\xi)\bar{p}^+}, \frac{\mathbf{\Delta}_\perp}{2}\right], \\ q &= \left[\eta(1+\xi)\bar{p}^+, \frac{-Q^2+\mathbf{\Delta}_\perp^2/4}{2\eta(1+\xi)\bar{p}^+}, \frac{\mathbf{\Delta}_\perp}{2}\right], \end{aligned} \tag{3}$$

where η equals $-x_{\rm Bj}$ up to corrections of order m^2/Q^2 and $\mathbf{\Delta}_\perp^2/Q^2$. Here, m denotes the mass of the proton. The average proton momentum is defined by

$$\bar{p} \,=\, \frac{1}{2}\,(p+p')\,, \tag{4}$$

and the skewness parameter ξ by

$$\xi \,=\, \frac{(p-p')^+}{(p+p')^+}\,. \tag{5}$$

In the photon–proton CM frame and for small $x_{\rm Bj}$, the skewness parameter is related to Bjorken-x by

$$\xi \,=\, \frac{x_{\rm Bj}}{2-x_{\rm Bj}} \simeq x_{\rm Bj}/2\,. \tag{6}$$

For Mandelstam t, given by

$$t \,=\, \Delta^2 \,=\, -\frac{4\xi^2 m^2 + \mathbf{\Delta}_\perp^2}{1-\xi^2}\,, \tag{7}$$

a minimal value is implied by the positivity of $\Delta_\perp^2$

$$-t_{\rm min} \,=\, 4m^2\frac{\xi^2}{1-\xi^2}\,. \tag{8}$$

Since we are interested in the region of small Bjorken-x and, hence, small skewness we will use $t_{\rm min} \simeq 0$ in the following. We also will neglect the proton and meson (m_V) masses in the kinematics.

Let us now consider the dynamics of vector-meson electroproduction in the kinematical regime specified above. The dominant contribution in this kinematical region comes from the emission and reabsorption of collinear gluons from the protons accompanied by $\gamma^* g \to V g$ scattering [9]. The neglect of an analogous quark contribution is justified by the fact that, at small $x_{\rm Bj}$, partons with small momentum fractions dominantly participate in hard meson electroproduction. Since, at small $-t$, the GPDs are expected to reflect the magnitudes of the usual parton distributions the gluon contribution should outweigh the quark one. This is in particular the case for electroproduction of ϕ mesons where only the small strange quark content of the proton is probed. Even for the production of ρ mesons the gluonic contribution seems to be still sizable for $x_{\rm Bj}$ as large as 0.1 as is indicated by the ratio of ϕ and ρ electroproduction cross sections [17].

The momenta of the gluons which, approximately, are collinearly emitted or absorbed by the protons, are parameterized as

$$k_g = \left[(\bar{x}+\xi)\bar{p}^+, \frac{\mathbf{\Delta}_\perp^2}{8(\bar{x}+\xi)\bar{p}^+}, -\mathbf{\Delta}_\perp/2\right],$$
$$k_g' = \left[(\bar{x}-\xi)\bar{p}^+, \frac{\mathbf{\Delta}_\perp^2}{8(\bar{x}-\xi)\bar{p}^+}, \ \mathbf{\Delta}_\perp/2\right]. \qquad (9)$$

In general the partons may have small virtualities of the order of $\mathbf{\Delta}_\perp^2$. As usual we have introduced an average parton momentum

$$\bar{k} \ = \ \frac{1}{2}(k_g + k_g'), \qquad (10)$$

and an average momentum fraction

$$\bar{x} \ = \ \bar{k}^+/\bar{p}^+. \qquad (11)$$

In order to facilitate comparison with other work we also provide the relations between the variables $\bar{x}$ and ξ and the usual Mandelstam variables for the hard subprocess. They read ($\hat{t} \simeq 0$)

$$\hat{s} = (q+k_g)^2 \simeq \frac{\bar{x}-\xi}{2\xi}\, Q^2,$$
$$\hat{u} = (q-k_g')^2 \simeq -\frac{\bar{x}+\xi}{2\xi}\, Q^2, \qquad (12)$$

and they are valid at large Q^2 and small ξ.

Radyushkin has calculated the asymptotically leading handbag contribution to meson electroproduction at small $x_{\rm Bj}$ [9]. As he showed, this contribution involves L $\to$ L transitions. Leaving aside for the time being a potential breakdown of factorization, Radyushkin's result can straightforwardly be generalized to other transitions [16, 18]. The crucial point in the derivation of the handbag amplitude is the use of light-cone gauge for the gluon field, $n \cdot A^a = 0$, where

$$n \ = \ [0, 1, \mathbf{0}_\perp], \qquad (13)$$

and a is a color label. This gauge allows us to express the gluon field by an integral over the gluon field strength tensor $G^a_{\nu\nu'}$ [9,19] (the limit $\tilde{\varepsilon} \to 0$ is to be understood):

$$A^a_\nu(z) \ = \ n^{\nu'} \int_0^\infty {\rm d}\sigma {\rm e}^{-\tilde{\varepsilon}\sigma}\, G^a_{\nu\nu'}(z+\sigma n). \qquad (14)$$

With the help of this expression one can replace the products of fields appearing in the perturbatively calculated amplitude for $\gamma^* p \to Vp$ by

$$A^{a\rho}(0)\, A^{a'\rho'}(\bar{z}) = \frac{\delta^{aa'}}{N_c^2-1}$$
$$\times \sum_{\lambda,\lambda'=\pm 1} \epsilon^\rho(k_g,\lambda)\, \epsilon^{*\rho'}(k_g',\lambda')$$
$$\times \int {\rm d}\sigma\, {\rm d}\sigma'\, {\rm e}^{-\tilde{\varepsilon}\sigma - \tilde{\varepsilon}'\sigma'}\, n^\omega\, n^{\omega'} G^a_{\nu\omega}(\sigma' n) G^a_{\nu'\omega'}(\bar{z}+\sigma n)$$
$$\times \epsilon^{*\nu}(k_g,\lambda)\, \epsilon^{\nu'}(k_g',\lambda'), \qquad (15)$$

where we have also made a helicity projection for the gluons. The use of the approximation (9) for the gluon momenta forces the relative distance of the fields on the light cone $z \to \bar{z} = [0, z_-, \mathbf{0}_\perp]$. The vectors $\epsilon(k_g,\lambda)$ and $\epsilon(k_g',\lambda')$ specify the polarization of the (on-shell) gluons, the corresponding momenta, k_g and k_g', are defined in (9). The first set of polarization vectors in (15) is to be used to contract the hard scattering kernel leading to gauge invariant parton-level helicity amplitudes $\mathcal{H}^V_{\mu'\lambda',\mu\lambda}$ for $\gamma^* g \to Vg$ (μ and μ' denote the helicities of γ^* and V, respectively). The contraction of the field strength tensors with the second set of polarization vectors leads to [20]

$$n^\omega n^{\omega'}\, G_{\nu\omega}(\sigma' n)\, G_{\nu'\omega'}(\bar{z}+\sigma n)\, \epsilon^{*\nu}(k_g,\lambda)\, \epsilon^{\nu'}(k_g',\lambda')$$
$$= \frac{1}{2}\, n^\omega n^{\omega'}\, G_{\nu\omega}(\sigma' n)\, G_{\nu'\omega'}(\bar{z}+\sigma n) \qquad (16)$$
$$\times \left[(-g_\perp^{\nu\nu'} + \lambda\, {\rm i}\epsilon_\perp^{\nu\nu'})\, \delta_{\lambda\lambda'} - t_\perp^{\nu\nu'}\, \delta_{\lambda-\lambda'}\right],$$

where

$$g_\perp^{11} = g_\perp^{22} = -\epsilon_\perp^{12} = \epsilon_\perp^{21} = -t_\perp^{11} = t_\perp^{22} = -1,$$
$$t_\perp^{12} = t_\perp^{21} = {\rm i}\lambda, \qquad (17)$$

while all other components of these tensors are zero. That only the transverse components in the contraction remain is a consequence of the chosen light-cone gauge and of the fact that the polarization vectors have zero plus-components in the CM frame we are working in.

Proton matrix elements of the gluon helicity non-flip contributions $g_\perp^{\mu\mu'}$ and ${\rm i}\epsilon_\perp^{\mu\mu'}$ in (16) define the unpolarized, $H^g(\bar{x},\xi,t)$ and $E^g(\bar{x},\xi,t)$, and the polarized, $\widetilde{H}^g(\bar{x},\xi,t)$ and $\widetilde{E}^g(\bar{x},\xi,t)$, gluon GPDs, respectively [9,10]. The proton matrix elements of these gluon field operators are related to the GPDs by

$$\langle p'\nu'| \sum_{a,a'} A^{a\rho}(0)\, A^{a'\rho'}(\bar{z}) |p\nu\rangle$$
$$= \frac{1}{2} \sum_{\lambda=\pm 1} \epsilon^\rho(k_g,\lambda)\, \epsilon^{*\rho'}(k_g',\lambda')$$
$$\times \int_0^1 \frac{{\rm d}\bar{x}}{(\bar{x}+\xi-{\rm i}\varepsilon)(\bar{x}-\xi+{\rm i}\varepsilon)}\, {\rm e}^{-{\rm i}(\bar{x}-\xi)p\cdot\bar{z}}$$
$$\times \left\{ \frac{\bar{u}(p'\nu')\, \not{n}\, u(p\nu)}{2\bar{p}\cdot n}\, H^g(\bar{x},\xi,t) \right.$$
$$+ \frac{\bar{u}(p'\nu')\, {\rm i}\sigma^{\alpha\beta}\, n_\alpha \Delta_\beta\, u(p\nu)}{4m\, \bar{p}\cdot n}\, E^g(\bar{x},\xi,t)$$
$$+ \lambda \frac{\bar{u}(p'\nu')\, \not{n}\gamma_5\, u(p\nu)}{2\bar{p}\cdot n}\, \widetilde{H}^g(\bar{x},\xi,t)$$
$$\left. + \lambda \frac{\bar{u}(p'\nu')\, n\cdot\Delta\, \gamma_5\, u(p\nu)}{4m\, \bar{p}\cdot n}\, \widetilde{E}^g(\bar{x},\xi,t) \right\}. \qquad (18)$$

Working out the spinor products one sees that for proton helicity non-flip the linear combinations [20]

$$H^g(\bar{x},\xi,t) - \frac{\xi^2}{1-\xi^2}\, E^g(\bar{x},\xi,t) \qquad (19)$$

and

$$\widetilde{H}^g(\bar{x},\xi,t) - \frac{\xi^2}{1-\xi^2}\,\widetilde{E}^g(\bar{x},\xi,t) \tag{20}$$

occur. Since we are interested in small ξ the E^g and $\widetilde{E}^g$ terms can safely be neglected in the expressions (19) and (20). For proton helicity flip, on the other hand, H^g and $\widetilde{H}^g$ do not contribute but only

$$-\kappa\,\frac{\sqrt{-t}}{2m}\,\frac{1}{1-\xi^2}\;E^g\;(\,2\nu\xi\widetilde{E}^g\,)\,, \tag{21}$$

where κ is a phase factor reading

$$\kappa = \frac{\Delta^1 + \mathrm{i}\Delta^2}{|\boldsymbol{\Delta}_\perp|}\,, \tag{22}$$

for proton momenta of the form (3).

The gluon helicity flip contribution in (16) which defines four more GPDs [21], will be neglected in the following since it is strongly suppressed at small $-t$. The mismatch between the proton and gluon helicities in the proton matrix elements has to be compensated by orbital angular momentum. For each unit of it a factor $\sqrt{-t}/m$ is picked up [21,22]. Further suppression comes from the subprocess amplitudes which behave as

$$\mathcal{H}^V_{\mu'\lambda',\mu\lambda} \sim \left(\sqrt{-t}/Q\right)^{|\mu-\lambda-\mu'+\lambda'|}\,, \tag{23}$$

at small $-t$ and from the fact that the amplitude $\mathcal{H}^V_{0-\lambda,\mu\lambda}$ vanishes for $\mu = \pm 1$ [18].

Combining all this, we finally obtain the helicity amplitudes for electroproduction of vector mesons [1]:

$$\begin{aligned}\mathcal{M}_{\mu'+,\mu+} = \frac{e}{2}\,\mathcal{C}_V \int_0^1 \frac{\mathrm{d}\bar{x}}{(\bar{x}+\xi)(\bar{x}-\xi+\mathrm{i}\varepsilon)} \\ \times\Big\{\big[\,\mathcal{H}^V_{\mu'+,\mu+} + \mathcal{H}^V_{\mu'-,\mu-}\,\big]\;H^g(\bar{x},\xi,t) \\ + \big[\,\mathcal{H}^V_{\mu'+,\mu+} - \mathcal{H}^V_{\mu'-,\mu-}\,\big]\;\widetilde{H}^g(\bar{x},\xi,t)\Big\}\end{aligned} \tag{24}$$

for proton helicity non-flip (explicit helicities are labelled by their signs) and for helicity flip

$$\begin{aligned}\mathcal{M}_{\mu'-,\mu+} = -\frac{e}{2}\,\mathcal{C}_V\,\kappa\,\frac{\sqrt{-t}}{2m} \int_0^1 \frac{\mathrm{d}\bar{x}}{(\bar{x}+\xi)(\bar{x}-\xi+\mathrm{i}\varepsilon)} \\ \times\Big\{\big[\,\mathcal{H}^V_{\mu'+,\mu+} + \mathcal{H}^V_{\mu'-,\mu-}\big]\,E^g(\bar{x},\xi,t) \\ + \big[\,\mathcal{H}^V_{\mu'+,\mu+} - \mathcal{H}^V_{\mu'-,\mu-}\big]\,\xi\widetilde{E}^g(\bar{x},\xi,t)\Big\}\,.\end{aligned} \tag{25}$$

The subprocess amplitudes, $\mathcal{H}^V$, are functions of Q^2, $\bar{x}$, ξ and t. The flavor weight factors, $\mathcal{C}_V$, read for ρ and ϕ mesons

$$\mathcal{C}_\rho = \frac{1}{\sqrt{2}}\,(e_u - e_d) = 1/\sqrt{2}\,; \qquad \mathcal{C}_\phi = e_s = -1/3\,, \tag{26}$$

[1] We note in passing that our helicities are light-cone helicities which naturally occur in the handbag approach. The difference to the usual CM frame helicities is of order $m\sqrt{-t}/W^2$ [21] and can be ignored in the kinematical region of interest in this work.

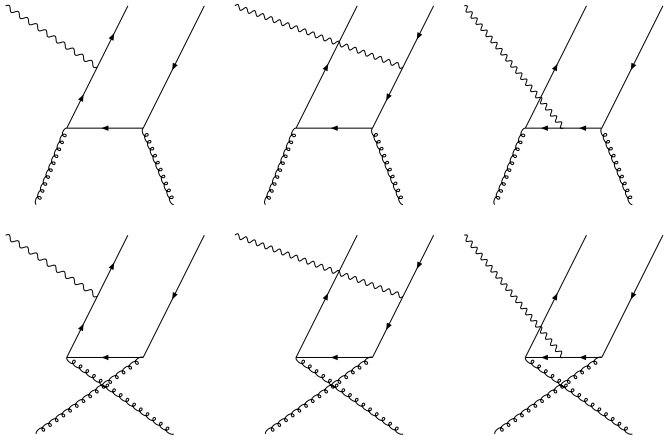

Fig. 2. Lowest order Feynman graphs for the subprocess $\gamma^* g \to Vg$

where e_i denotes the quark charge in units of the positron charge e. The remaining helicity amplitudes are obtained with the help of parity invariance,

$$\mathcal{M}_{-\mu'-\nu',-\mu-\nu} = (-1)^{\mu-\nu-\mu'+\nu'}\;\mathcal{M}_{\mu'\nu',\mu\nu}\,. \tag{27}$$

An analogous relation holds for the subprocess amplitudes.

3 The partonic subprocess $\gamma^* g \to Vg$

The parton-level amplitudes for the subprocess $\gamma^* g \to Vg$ are calculated from the Feynman graphs shown in Fig. 2; the outgoing $q\bar{q}$ pair is to be combined into the vector meson regarding its quantum numbers. This is conveniently done by means of a covariant spin wavefunction. As is well known from analyses of hadron form factors at large momentum transfer, leading-twist perturbative calculations are instable in the end-point regions since the contributions from large transverse separations, **b**, of quark and antiquark forming the meson are not sufficiently suppressed. In order to eliminate that defect Li and Sterman [23] retained the quark transverse degrees of freedoms and took into account Sudakov suppressions. Including, in addition, meson wavefunctions with their intrinsic transverse momentum dependence instead of distribution amplitudes [24], the perturbative contributions to form factors can reliably and self-consistently be calculated, the end-point regions are strongly damped.

Since the subprocess $\gamma^* g \to Vg$ bears resemblance to the meson form factors it is tempting to apply this so-called modified perturbative approach also here in order to suppress the contributions from the soft end-point regions and, simultaneously, to regularize this way infrared divergencies that may occur in the T $\to$ L and T $\to$ T amplitudes [16]. The modified perturbative approach applied to the subprocess, is, to some extent, similar to the mechanism proposed in [6] for the suppression of the leading-twist gluon contribution to hard meson electroproduction.

It is however to be stressed that in [6] the leading $\ln(1/x_{\rm Bj})$ approximation of [4] has been utilized.

Let us now turn to the description of the soft $q\bar{q} \to V$ transtion matrix element. We start from a frame where the hadron rapidly moves along the 3-direction ($q' = [0, q'^-, \mathbf{0}_\perp]$ with $q'^- \simeq Q/(2\sqrt{\xi})$). This frame is termed the hadron-out one. The momenta of the quark and the antiquark which form the valence Fock state of the meson are parameterized as

$$q_1^\mu \,=\, \tau q'^\mu + k_1^\mu\,, \qquad q_2^\mu \,=\, \bar\tau q'^\mu + k_2^\mu\,, \tag{28}$$

where

$$k_1 \,=\, [k_1^+, 0, \mathbf{k}_{1\perp}]\,, \qquad k_2 \,=\, [k_2^+, 0, \mathbf{k}_{2\perp}]\,. \tag{29}$$

The variables τ and $\bar\tau$ are the usual fractions of the light-cone minus-component of the meson's momentum the constituents carry. Momentum conservation provides the constraints

$$\bar\tau \,=\, 1-\tau\,, \qquad \mathbf{k}_{2\perp} \,=\, -\mathbf{k}_{1\perp} \equiv -\mathbf{k}_\perp\,. \tag{30}$$

It can be shown [25] that the variables $\tau, \bar\tau$ and $\mathbf{k}_\perp$ are invariant under all kinematical Poincaré transformations, i.e. under boosts along and rotations around the 3-direction as well as under transverse boosts. Moreover – and this is an important point – the light-cone wavefunction associated with the valence Fock state, $\Psi_V = \Psi_V(\tau, \mathbf{k}_\perp)$, is independent of the hadron's momentum and is invariant under these kinematical transformations too. The light-cone wavefunction may differ for longitudinally and transversally polarized vector mesons [26].

As is customary in the parton approach we neglect the binding energy. That possibly crude approximation can be achieved by putting the individual k_j^+ components to zero. In fact starting from a parameterisation of the various momenta in the meson's rest frame and boosting to the hadron-out frame, one sees that the k_j^+ components are of order m_V^2/q'^-. The plus-component of the difference of the momenta

$$K \,=\, \frac{1}{2}\,(k_1 - k_2)\,, \tag{31}$$

is zero with this choice of k_j^+ components and, hence,

$$K \,=\, [0, 0, \mathbf{k}_\perp]\,, \tag{32}$$

and $q'\cdot K = 0$. The quarks are treated as massless in the hadron-out frame; they are not strictly on-shell.

It is convenient to couple the spinors representing quark and antiquark in a covariant spin wavefunction for the vector meson. The Dirac indices of it (omitted for convenience) are to be contracted with the corresponding ones of the hard scattering kernel (see below). For the construction of the spin wave function we adapt the method presented in [27] (see also [28]) straightforwardly to vector mesons. The product of spinors $v(q_2)\bar u(q_1)$ is boosted to the hadron's rest frame, coupled there into the quantum numbers of the vector meson and boosted back to hadron-out frame. Separating terms with and without K and neglecting terms $\propto K^2$, one arrives at

$$\mathit{\Gamma}_V \,=\, \mathit{\Gamma}_{V0} + \mathit{\Delta\Gamma}_{V\alpha} K^\alpha\,, \tag{33}$$

where

$$\mathit{\Gamma}_{V0} \,=\, \frac{1}{\sqrt{2}}\,(\not{q}' + m_V)\not{\epsilon}_V\,, \qquad \mathit{\Delta\Gamma}_\alpha \,=\, \frac{1}{M_V}\,\{\mathit{\Gamma}_{V0}, \gamma_\alpha\}\,. \tag{34}$$

The polarization state of the meson is described by the vector ϵ. The soft physics parameter M_V is of order m_V; its model dependence results from the specific treatment of the quarks in the meson's rest frame. In the following we will use $M_V = m_V$ for simplicity but we will comment on other choices of it.

Since the anticommutator $\{\mathit{\Gamma}_{V0}, \not{q}'\}$ is zero the 4-vector K is only determined up to a multiple of the meson momentum. This property can be used to identify K^μ, given in (32), with the quark–antiquark relative momentum

$$K^\mu \to \frac{1}{2}(q_1 - q_2)\,, \tag{35}$$

where the parton momenta, q_i, are defined in (28). This choice, although not forced, is very convenient. Its main advantage is that K^μ now represents one unit of orbital angular momentum in a covariant manner [27]. As discussed in this article, the relative momentum (35) is a 4-transverse vector defined by $K_\perp^\mu = K^\mu - q'\cdot K/m_V^2\, q'^\mu$. In the hadron-out frame and up to corrections of order m_V^2/q'^-, $K_\perp = K$. In the meson's rest frame on the other hand, clearly $K_\perp = (0, \boldsymbol{k})$, and one has an object transforming as a 3-vector under the three-dimensional rotation group $O(3)$.

One of the basis ingredients of the hard scattering picture is the collinear approximation which says that all constituents move along the same direction as their parent hadron up to a scale of the order of the Fermi motion $\langle \mathbf{k}_\perp^2\rangle$ which typically amounts to a few 100 MeV. The (nearly) collinear kinematics justifies an expansion of the spin wavefunction upon a power series in $\mathbf{k}_\perp$ or, in order to retain a covariant formulation, in K^μ. Up to terms linear in K^μ this expansion is given above for vector mesons.

The transformation from the hadron-out frame to our CM frame, where the meson momentum has a transverse component $-\mathbf{\Delta}_\perp/2$, is executed by a transverse boost (cf. e.g. [29]) that leaves the minus-component of any momentum vector a unchanged and which involves a parameter d^- and a transverse vector $\mathbf{d}_\perp$; it is defined by

$$\begin{aligned}&[\,a^+, a^-, \mathbf{a}_\perp] \\ &\longrightarrow \left[a^+ - \frac{\mathbf{a}_\perp\cdot\mathbf{d}_\perp}{d^-} + \frac{a^-\,\mathbf{d}_\perp^2}{2\,(d^-)^2}\,,\, a^-\,,\, \mathbf{a}_\perp - \frac{a^-}{d^-}\,\mathbf{d}_\perp\right].\end{aligned} \tag{36}$$

The transverse boost is one of the kinematical Poincaré transforms that leaves the hadron wavefunction invariant. Taking for the parameters $d^- = q'^-$ and $\mathbf{d}_\perp = \mathbf{\Delta}_\perp/2$, we readily find from (28) the expressions for the quark momenta and the relative momentum in the CM frame.

Provided the quark transverse momenta are taken into account, the general structure of the $\gamma^* g \to V g$ amplitude is

$$\mathcal{H}^V = \int \frac{\mathrm{d}\tau \mathrm{d}^2\mathbf{k}_\perp}{16\pi^3} \Psi_V(\tau, k_\perp^2)\, \mathrm{Tr}\left[\Gamma_V\, T_\mathrm{H}\right] . \qquad (37)$$

The hard scattering kernel, $T_\mathrm{H} = T_\mathrm{H}(\tau, \bar{x}, Q^2, K, t)$, can be written as follows:

$$T_\mathrm{H} = T_0(\tau, \bar{x}, Q^2, k_\perp^2, t) + \Delta T_\mu(\tau, \bar{x}, Q^2, k_\perp^2, t) K^\mu + \ldots \qquad (38)$$

Terms $\propto K^\mu K^\nu$ (and higher) in the numerator are neglected while, in the spirit of the modified perturbative approach [23], the $k_\perp^2$ terms in the denominators are kept. Inserting (38) as well as the spin wavefunction (33) into (37), one obtains

$$\begin{aligned}\mathcal{H}^V = &\int \frac{\mathrm{d}\tau \mathrm{d}^2\mathbf{k}_\perp}{16\pi^3} \Psi_V(\tau, k_\perp^2) \\ &\times \mathrm{Tr}\left[\Gamma_{V0}\, T_0 + \Delta\Gamma_{V\alpha}\, T_0\, K^\alpha \right. \\ &\left. + \Gamma_0\, \Delta T_\beta\, K^\beta + \Delta\Gamma_{V\alpha}\, \Delta T_\beta\, K^\alpha\, K^\beta + \ldots\right] . \end{aligned} \qquad (39)$$

Obviously, the terms $\propto K^\mu$ integrate to zero while the $K^\mu K^\nu$ term survives the $k_\perp$-integration. Hence,

$$\begin{aligned}\mathcal{H}^V = &\int \mathrm{d}\tau \frac{\mathrm{d}k_\perp^2}{16\pi^2} \Psi_V(\tau, k_\perp^2) \\ &\times \mathrm{Tr}\left\{\Gamma_{V0} T_0 - \frac{1}{2} k_\perp^2 g_\perp^{\alpha\beta}\, \Delta\Gamma_{V\alpha}\, \Delta T_\beta + \ldots\right\} , \end{aligned} \qquad (40)$$

where $g_\perp$ is the transverse metric tensor defined in (17). In order to simplify matters we only take into account the first non-zero term in this expansion for each amplitude, i.e. we neglect any correction of order m_V or $k_\perp^2$ to its leading term[2]. As we said above we however retain the $k_\perp^2$ terms in the denominators of the propagators. Moreover, any t dependence of the subprocess amplitudes is ignored except the factors of $\sqrt{-t}$ required by angular momentum conservation. This is justified in the small t region we are interested in.

For longitudinally polarized vector mesons the first term in (40) contributes, the other term represents a $k_\perp^2$ correction to it which we, according to our strategy, neglect as well as all other terms indicated by the ellipses. For transversely polarized mesons, on the other hand, the first term in (40) disappears since the number of γ matrices in the trace is odd[3]. The second term in (40), $\propto k_\perp^2$, contributes in this case; it scales as $\propto k_\perp^2/(m_V Q)$; see (34). Combining this property with the behavior of the subprocess amplitudes near the forward direction (23) and utilizing the fact that $\langle k_\perp^2\rangle^{1/2}/m_V$ is of order 1, the various photon–meson transitions respect the following hierarchy:

$$\begin{aligned} \mathrm{L} \to \mathrm{L}: &\qquad \mathcal{H}^V_{0\,\lambda,0\,\lambda} \propto 1 , \\ \mathrm{T} \to \mathrm{L}: &\qquad \mathcal{H}^V_{0\,\lambda,+\lambda} \propto \frac{\sqrt{-t}}{Q} , \\ \mathrm{T} \to \mathrm{T}: &\qquad \mathcal{H}^V_{+\lambda,+\lambda} \propto \frac{\langle k_\perp^2\rangle^{1/2}}{Q} , \\ \mathrm{L} \to \mathrm{T}: &\qquad \mathcal{H}^V_{+\lambda,0\,\lambda} \propto \frac{\sqrt{-t}}{Q}\, \frac{\langle k_\perp^2\rangle^{1/2}}{Q} , \\ \mathrm{T} \to -\mathrm{T}: &\qquad \mathcal{H}^V_{-\lambda,+\lambda} \propto \frac{-t}{Q^2}\, \frac{\langle k_\perp^2\rangle^{1/2}}{Q} . \end{aligned} \qquad (41)$$

This hierarchy propagates to the proton non-flip amplitudes for the full process and justifies the neglect of $\mathrm{L} \to \mathrm{T}$ and $\mathrm{T} \to -\mathrm{T}$ transitions in the analysis. The amplitudes for proton helicity flip have an extra factor $\sqrt{-t}/m$; see (25). Our interest in this work is focused on unpolarized protons. In the corresponding cross sections there is no interference between flip and non-flip amplitudes. Hence, proton flip is suppressed by a factor of t and since there is no theoretical or phenomenological indication that $|E^g|$ is much larger than H^g [22], neglected by us. Information on the proton flip amplitudes may be extracted from the data on meson electroproduction with polarized protons. As a last simplification we neglect contributions from $\widetilde{H}^g$ in the evaluation of the amplitudes. Since in the forward limit, $\xi, t \to 0$, H^g and $\widetilde{H}^g$ reduce to $\bar{x} g(\bar{x})$ and $\bar{x} \Delta g(\bar{x})$, respectively, it is plausible that the relative size of Δg and g is reflected in that of $\widetilde{H}^g$ and H^g at small ξ and $-t$. Since $|\Delta g(\bar{x})|$ is much smaller than $g(\bar{x})$ the contribution from $\widetilde{H}^g$ can safely be neglected. The model GPDs we are going to construct in Sect. 5 do indeed respect this assertion. As a consequence of parity invariance, see (24) and (27), there is anyway no contribution from the GPD $\widetilde{H}^g$ to the most important amplitude, $\mathrm{L} \to \mathrm{L}$. Care is required for observables for which the contribution from H^g partially if not totally cancels. An example of such an observable is the correlation of the electron and proton helicities. We will comment on this observable in Sect. 8.

The hard scattering amplitudes for the three helicity configurations we keep in our analysis are to be calculated from the Feynman graphs shown in Fig. 2. The results for the relevant sums and differences of positive and negative gluon helicities can be cast into the following form:

$$\begin{aligned}\mathcal{H}^V_{\mu'+,\mu+} \pm \mathcal{H}^V_{\mu'-,\mu-} = &\frac{8\pi\alpha_\mathrm{s}(\mu_\mathrm{R})}{\sqrt{2N_c}} \\ \times \int_0^1 \mathrm{d}\tau &\int \frac{\mathrm{d}^2\mathbf{k}_\perp}{16\pi^3} \Psi_{V\mu'}(\tau, k_\perp^2)\, (\bar{x}^2 - \xi^2)\, f^\pm_{\mu'\mu} D , \end{aligned} \qquad (42)$$

where the product of propagator denominators reads

$$\begin{aligned} D^{-1} = &\left(k_\perp^2 + \bar{\tau}\, Q^2\right)\, \left(k_\perp^2 + \tau\, Q^2\right) \\ &\times \left(k_\perp^2 - \bar{\tau}\, (\bar{x} - \xi)\, Q^2/(2\,\xi) - \mathrm{i}\varepsilon\right) \\ &\times \left(k_\perp^2 + \bar{\tau}\, (\bar{x} + \xi)\, Q^2/(2\,\xi)\right) \\ &\times \left(k_\perp^2 + \tau\, (\bar{x} + \xi)\, Q^2/(2\,\xi)\right) \\ &\times \left(k_\perp^2 - \tau\, (\bar{x} - \xi)\, Q^2/(2\,\xi) - \mathrm{i}\varepsilon\right) . \end{aligned} \qquad (43)$$

[2] Note that the hard scattering kernel T_H does not depend on the vector-meson mass; it occurs through the spin wavefunction.

[3] We remind the reader that for longitudinally polarized vector mesons $\epsilon(0) = q'/m_V$ up to corrections of order m_V/q'^-.

Here, N_C denotes the number of colors. The functions $f^{\pm}_{\mu'\mu}$ read

$$
\begin{aligned}
f^{+}_{00} &= Q^{11}\,(\bar{x}^2-\xi^2)\,\frac{\tau^2\bar{\tau}^2}{4\,\xi^4}\,,\\
f^{+}_{0+} &= Q^{10}\,\sqrt{\frac{-t}{2}}\,(\bar{x}^2-\xi^2)^{1/2}\,\frac{\tau^2\bar{\tau}^2}{2\xi^3}\,,\\
f^{+}_{++} &= -\frac{k_\perp^2}{m_V}\,Q^{10}\,\frac{\tau\bar{\tau}}{8\,\xi^4}\,[\bar{x}^2-\xi^2-2\tau\bar{\tau}\,(\bar{x}^2+\xi^2)]\,,\\
f^{-}_{++} &= \frac{k_\perp^2}{m_V}\,Q^{10}\,\frac{\tau^2\bar{\tau}^2}{2\,\xi^3}\,\bar{x}\,,\\
f^{-}_{00} &= f^{-}_{0+} \,=\, 0\,.
\end{aligned}
\tag{44}
$$

Following [23], we retain $k_\perp^2$ terms in the denominators of the propagators (43). These terms play an important role since they compete with terms $\propto \tau(\bar{\tau})Q^2$ which become small in the end-point regions where either τ or $\bar{\tau}$ tends to zero. They lead to the suppression of contributions with large quark–antiquark separations as we mentioned above.

In collinear approximation and utilizing distribution amplitudes up to twist-3 accuracy the subprocess amplitudes for $\mathrm{T}\to\mathrm{T}$ transitions are infrared divergent, signaling the breakdown of factorization [16]. Neglecting transverse momenta in (43), one finds

$$
\begin{aligned}
&\mathcal{H}^V_{++,++} + \mathcal{H}^V_{+-,+-}\\
&\sim \int \frac{\mathrm{d}\tau}{\tau^2\bar{\tau}^2}\,\frac{\bar{x}^2-\xi^2-2\tau\bar{\tau}(\bar{x}^2+\xi^2)}{\bar{x}^2-\xi^2}\\
&\qquad\times\int \mathrm{d}k_\perp^2\,k_\perp^2\,\Psi_{V\mathrm{T}}(\tau,k_\perp^2)\,.
\end{aligned}
\tag{45}
$$

Assuming for instance a Gaussian wavefunction, $\Psi_{V\mathrm{T}}\sim \exp\,[a_{V\mathrm{T}}^2 k_\perp^2/(\tau\bar{\tau})]$, an ansatz that has been shown to work successfully in many cases (see for instance [24]) and will be used by us in the numerical analysis of meson electroproduction, we find that in fact the τ integral is regular. As pointed out in [16], the $\bar{x}$ integral in (24) may not exist due to the double pole $(\bar{x}-\xi+\mathrm{i}\varepsilon)^{-2}$ occurring. Whether or not this happens depends on the properties of the GPDs. In Sect. 5 we will take up this problem again.

One may also consider a transverse momentum dependence of the GPDs. That issue has been investigated in [30] for meson electroproduction at intermediate values of x_{Bj}. In this kinematical region the emission and reabsorption of quarks from the proton dominates. We however think that the $k_\perp$ dependence of the GPDs is of minor importance. In contrast to the meson where the hard process enforces the dominance of the compact valence Fock state of the meson, all proton Fock states contribute to the GPDs at small $-t$ [20,22]. If the gluons are distributed in the proton like the quarks, an assumption that is supported by the slope of the diffraction peak in elastic proton-proton scattering, the $k_\perp$ dependence of the GPD H^g should roughly reflect the charge radius of the proton ($\langle k_\perp^2\rangle^{1/2}\simeq 200\,\mathrm{MeV}$). Consequently, we expect H^g to be only mildly dependent on the transverse momentum, a potential effect we neglect.

4 The impact parameter space

Transverse momenta in the subprocess amplitudes, see Sect. 3, imply finite quark–antiquark separations in the configuration space which are accompanied by gluon radiation. On the grounds of previous work by Collins and Soper [31], Sterman and collaborators [23] calculated this radiation to next-to-leading-log approximation using resummation techniques and having recourse to the renormalization group. The result is a Sudakov factor which suppresses large quark–antiquark separations and which we also have to take into account in our analysis in order to have consistency with the retention of the transverse degrees of freedom. Since the Sudakov factor is given in the transverse separation or impact parameter space – only in this space the gluonic radiative corrections exponentiate – we have to work in this space.

The two-dimensional Fourier transformation between the canonical conjugated $\mathbf{b}$ and $\mathbf{k}_\perp$ spaces is defined by

$$
\hat{f}(\mathbf{b}) \,=\, \frac{1}{(2\pi)^2}\int \mathrm{d}^{\,2}\,\mathbf{k}_\perp\,\exp\,[-\mathrm{i}\,\mathbf{k}_\perp\cdot\mathbf{b}\,]\,f(\mathbf{k}_\perp)\,. \tag{46}
$$

For the meson wavefunctions we adopt the same Gaussian parameterization as is used for the pion [24,32]:

$$
\Psi_{Vi}(\tau,k_\perp^2) \,=\, 8\pi^2\sqrt{2N_c}\,f_{Vi}\,a_{Vi}^2\,\exp\left[-a_{Vi}^2\,\frac{\mathbf{k}_\perp^{\,2}}{\tau\bar{\tau}}\right] \tag{47}
$$

($i=\mathrm{L},\mathrm{T}$), which strictly speaking represents full wavefunctions with their perturbative tails removed. Transverse momentum integration of these wavefunctions leads to the associated distribution amplitudes which represent the soft hadronic matrix elements entering the calculations within the collinear factorization approach. Actually, the wavefunction (47) leads to the so-called asymptotic meson distribution amplitude:

$$
\Phi_{\mathrm{AS}} \,=\, 6\tau\bar{\tau}\,. \tag{48}
$$

For the decay constants $f_{V\mathrm{L}}$ of longitudinally polarized vector mesons we take the values [33]

$$
f_{\rho\,\mathrm{L}} \,=\, 0.216\,\mathrm{GeV}\,,\qquad f_{\phi\,\mathrm{L}} \,=\, 0.237\,\mathrm{GeV}\,. \tag{49}
$$

The decay constants for transversely polarized vector mesons are almost unknown. The only available information comes from QCD sum rules. In [26] $f_{\rho\,\mathrm{T}}$ has been estimated to be $(160\pm 10)\,\mathrm{MeV}$. We actually fit these decay constants to experiment. Identifying for instance the soft parameter M_V in the spin wavefunction with the meson mass, we obtain

$$
f_{\rho\,\mathrm{T}} \,=\, 0.250\,\mathrm{GeV}\,,\qquad f_{\phi\,\mathrm{T}} \,=\, 0.275\,\mathrm{GeV}\,. \tag{50}
$$

Choosing M_V to be smaller than the meson mass results in smaller values of the decay constants $f_{V\,\mathrm{T}}$. The transverse size parameters $a_{V\mathrm{L}}$ are fixed by the requirement of equal probabilities for the vector meson and pion valence Fock states, namely 0.25. This leads to

$$
a_{\rho\,\mathrm{L}} \,=\, 0.52\,\mathrm{GeV}^{-1}\,,\qquad a_{\phi\,\mathrm{L}} \,=\, 0.45\,\mathrm{GeV}^{-1}\,. \tag{51}
$$

The transverse size parameters for transversely polarized vector mesons are adjusted to experiment. The numerical results we are going to present below are obtained with

$$a_{\rho\,\mathrm{T}} \,=\, 0.65\,\mathrm{GeV}^{-1}\,, \qquad a_{\phi\,\mathrm{T}} \,=\, 0.60\,\mathrm{GeV}^{-1}\,. \tag{52}$$

With the parameter values quoted in (49) and (51) the RMS transverse momenta, evaluated from (47), amount to 0.61 GeV and 0.67 GeV for the longitudinally polarized ρ and ϕ mesons, respectively. These values are much larger than the one for the proton RMS transverse momentum.

The Fourier transform of the meson wavefunction (47) reads

$$\hat{\Psi}_{Vi}(\tau,b^2) \,=\, 2\pi\,\frac{f_{Vi}}{\sqrt{2N_c}}\,\Phi_{\mathrm{AS}}(\tau)\,\exp\left[-\tau\bar{\tau}\frac{b^2}{4a_{Vi}^2}\right]. \tag{53}$$

The product of the propagator denominators D (43) can be decomposed into single-pole terms which are either of the form

$$T_1 \,=\, \frac{1}{\mathbf{k}_\perp^2 + d_1 Q^2}\,, \tag{54}$$

or

$$T_2 \,=\, \frac{1}{\mathbf{k}_\perp^2 - d_2(\bar{x}-\xi)Q^2 - \mathrm{i}\hat{\varepsilon}}\,. \tag{55}$$

where $d_i \geq 0$. The Fourier transforms of these pole terms can readily be obtained:

$$\begin{aligned}
\hat{T}_1 &= \frac{1}{2\pi}\,K_0(\sqrt{d_1}bQ)\,,\\
\hat{T}_2 &= \frac{1}{2\pi}\,K_0\left(\sqrt{d_2(\xi-\bar{x})}bQ\right)\,\theta(\xi-\bar{x})\\
&\quad +\frac{\mathrm{i}}{4}\,H_0^{(1)}\left(\sqrt{d_2(\bar{x}-\xi)}bQ\right)\,\theta(\bar{x}-\xi)\,,
\end{aligned} \tag{56}$$

where K_0 and $H_0^{(1)}$ are the zeroth order modified Bessel function of the second kind and the Hankel function, respectively.

Putting all this together and including the Sudakov factor, $\exp[-S(\tau,b,Q)]$, the gluonic contributions to the helicity amplitudes for vector-meson electroproduction read

$$\begin{aligned}
\mathcal{M}_{\mu'+,\mu+} &= \mathcal{M}^H_{\mu'+,\mu+} + \mathcal{M}^{\widetilde{H}}_{\mu'+,\mu+},\\
\mathcal{M}^H_{\mu'+,\mu+} &= \frac{e}{\sqrt{2N_c}}\mathcal{C}_V\int \mathrm{d}\bar{x}\mathrm{d}\tau f^+_{\mu'\mu}H^g(\bar{x},\xi,t)\\
&\quad\times\int \mathrm{d}^{\,2}\mathbf{b}\hat{\Psi}_{V\mu'}(\tau,b^2)\hat{D}(\tau,Q,b)\,\alpha_{\mathrm{s}}(\mu_{\mathrm{R}})\\
&\qquad\times\exp\left[-S(\tau,b,Q)\right],\\
\mathcal{M}^{\widetilde{H}}_{\mu'+,\mu+} &= \frac{e}{\sqrt{2N_c}}\mathcal{C}_V\int \mathrm{d}\bar{x}\mathrm{d}\tau f^-_{\mu'\mu}\widetilde{H}^g(x,\xi,t)\\
&\quad\times\int \mathrm{d}^{\,2}\mathbf{b}\hat{\Psi}_{V\mu'}(\tau,b^2)\hat{D}(\tau,Q,b)\,\alpha_{\mathrm{s}}(\mu_{\mathrm{R}})\\
&\qquad\times\exp\left[-S(\tau,b,Q)\right],
\end{aligned} \tag{57}$$

which is the **b**-space version of the amplitude (24). The functions D and $f^{\pm}_{\mu'\mu}$ are given in (43) and (44). Since the Fourier transformed wavefunctions, the product of propagator denominators as well as the Sudakov factor, only depend on b, the angle integration in the last integral is trivial and a three-dimensional integral ($\mathrm{d}\bar{x}\mathrm{d}\tau b\,\mathrm{d}b$) remains to be evaluated numerically. Parity invariance (27) leads to the following relations among the amplitudes[4]:

$$\begin{aligned}
\mathcal{M}^H_{++,++} &= \mathcal{M}^H_{-+,-+}\,, \qquad \mathcal{M}^H_{0+,++} \,=\, -\mathcal{M}^H_{0+,-+}\,,\\
\mathcal{M}^{\widetilde{H}}_{++,++} &= -\mathcal{M}^{\widetilde{H}}_{-+,-+}\,, \qquad \mathcal{M}^{\widetilde{H}}_{0+,++} \,=\, \mathcal{M}^{\widetilde{H}}_{0+,-+}\,,
\end{aligned} \tag{58}$$

The Sudakov exponent S in (57) is given by [23]

$$S(\tau,b,Q) = s(\tau,b,Q) + s(\bar{\tau},b,Q) - \frac{4}{\beta_0}\ln\frac{\ln\left(\mu_{\mathrm{R}}/\Lambda_{\mathrm{QCD}}\right)}{\hat{b}}\,, \tag{59}$$

where a Sudakov function s occurs for each quark line entering the meson, and the abbreviation

$$\hat{b} \,=\, -\ln\left(b\Lambda_{\mathrm{QCD}}\right), \tag{60}$$

is used. The last term in (59) arises from the application of the renormalization group equation ($\beta_0 = 11-\frac{2}{3}n_f$) where n_f is the number of active flavors, taken to be 3. A value of 220 MeV for Λ_{QCD} is used here and in the evaluation of α_{s} from the one-loop expression. The renormalization scale μ_{R} is taken to be the largest mass scale appearing in the hard scattering amplitude, i.e. $\mu_{\mathrm{R}} = \max\left(\tau Q, \bar{\tau}Q, 1/b\right)$. For small b there is no suppression from the Sudakov factor; as b increases, the Sudakov factor decreases, reaching zero at $b = 1/\Lambda_{\mathrm{QCD}}$. For even larger b the Sudakov is set to zero[5]. The Sudakov function s reads

$$s(\tau,b,Q) = \frac{8}{3\beta_0}\left(\hat{q}\ln\left(\frac{\hat{q}}{\hat{b}}\right) - \hat{q} + \hat{b}\right) + \text{NLL-terms}\,, \tag{61}$$

where

$$\hat{q} \,=\, \ln\left(\tau Q/(\sqrt{2}\Lambda_{\mathrm{QCD}})\right). \tag{62}$$

Actually we do not use the explicit form of the next-to-leading-log corrections quoted in [23] but those given in [35]. The latter ones contain some minor corrections which are hardly relevant numerically. Due to the properties of the Sudakov factor any contribution to the amplitudes is damped asymptotically, i.e. for $\ln(Q^2/\Lambda^2_{\mathrm{QCD}}) \to \infty$, except those from configurations with small quark–antiquark separations. b plays the role of an infrared cut-off; it sets up the interface between non-perturbative soft gluon contributions – still contained in the hadronic wavefunction – and perturbative soft gluon contributions accounted for by the Sudakov factor.

[4] The same relations as for the H^g terms also hold for the t-channel exchange of a particle with natural parity, $P = (-1)^J$. The relations for the $\widetilde{H}^g$ terms in (57) corresponds to those obtained for an unnatural parity exchange [34].

[5] The definition of the Sudakov factor is completed by the following rules [23]: $\exp\left[-S\right] = 1$ if $\exp\left[-S\right] \geq 1$, $\exp\left[-S\right] = 0$ if $b \geq 1/\Lambda_{\mathrm{QCD}}$ and $s(\beta,b,Q) = 0$ if $b \leq \sqrt{2}/\beta Q$.

5 Modeling the GPDs

In order to calculate the electroproduction amplitudes (24) we still need the gluon GPDs. A model for them can be constructed with the help of double distributions [36] which guarantee polynomiality of the GPDs. The gluonic double distribution $f(\beta,\alpha,t\simeq 0)$ is customarily parameterized as

$$f(\beta,\alpha,t\simeq 0) = g(\beta)\,\frac{\Gamma(2n+2)}{2^{2n+1}\,\Gamma^2(n+1)}\,\frac{[(1-|\beta|)^2-\alpha^2]^n}{(1-|\beta|)^{2n+1}}\,, \tag{63}$$

where $g(x)$ is the usual gluon distribution. Its definition is extended to negative β by

$$g(-\beta) \,=\, -g(\beta)\,. \tag{64}$$

A popular choice of n is 1 for quarks and 2 for gluons. This is motivated by the interpretation of the α dependence like a meson distribution amplitude for hard exclusive processes. The cases $n=1$ and 2 correspond to the asymptotic behavior of a quark distribution amplitude $\propto(1-\alpha^2)$ and for gluons $\propto(1-\alpha^2)^2$, respectively. This correspondence is not demanded by theory. Therefore, we will consider both the cases, $n=1$ and 2, for the construction of the gluon GPD. A parameterization of the t dependence of f is difficult. The multiplication of f as given in (63) by a t-dependent form factor, although frequently used in default of a better idea, is unsatisfactory. Parameterizations of the GPDs [37,38] as well as results from lattice QCD [39] revealed that a factorization of f in β,α on the one hand and in t on the other hand is most likely incorrect. Fortunately, the knowledge of the GPDs at $t\simeq 0$ suffices for our purposes as will become clear in Sect. 6.

According to [36], the GPD H^g is related to the double distribution by (since we will only work with GPDs at $t\simeq 0$ we omit the variable t in the GPDs in the following)

$$\begin{aligned} H^g(\bar{x},\xi) &= \left[\Theta(0\le\bar{x}\le\xi)\int_{x_3}^{x_1}\mathrm{d}\beta+\Theta(\xi\le\bar{x}\le 1)\int_{x_2}^{x_1}\mathrm{d}\beta\right] \\ &\quad\times\frac{\beta}{\xi}\,f\left(\beta,\alpha=\frac{\bar{x}-\beta}{\xi}\right) \\ &\quad+\xi\,D^g\left(\frac{\bar{x}}{\xi}\right)\,. \end{aligned} \tag{65}$$

The definition of H^g is completed by noting that it is an even function of $\bar{x}$:

$$H^g(-\bar{x},\xi) \,=\, H^g(\bar{x},\xi)\,. \tag{66}$$

The integration limits in (65) are given by

$$x_1 \,=\, \frac{\bar{x}+\xi}{1+\xi}\,,\quad x_2 \,=\, \frac{\bar{x}-\xi}{1-\xi}\,,\quad x_3 \,=\, \frac{\bar{x}-\xi}{1+\xi}\,. \tag{67}$$

The limit $x_1(x_2)$ is the momentum fraction the emitted (reabsorbed) gluon carries with respect to the incoming (outgoing) proton. The last term in the definition (65) is the so-called D-term [40]. Its support is the region $-\xi\le\bar{x}\le\xi$ and it ensures the correct polynomiality property of the GPD. Since the D term is $\propto\xi$ and our interest lies in small skewness, we neglect it.

We take the gluon distribution from the NLO CTEQ5M results [41] and use an interpolation of it which has been proposed in [42] and which is valid in the range $Q_0^2=4\,\mathrm{GeV}^2\le Q^2\le 40\,\mathrm{GeV}^2$,

$$\beta g(\beta) \,=\, \beta^{-\delta(Q^2)}\,(1-\beta)^5\,\sum_{i=0}^{2} c_i\,\beta^{i/2}\,, \tag{68}$$

where

$$\begin{aligned} &c_0 = 1.94\,,\quad c_1 \,=\, -3.78+0.24\ln\left(Q^2/Q_0^2\right)\,, \\ &c_2 = 6.79-2.13\ln\left(Q^2/Q_0^2\right)\,. \end{aligned} \tag{69}$$

This is a very good approximation to the CTEQ gluon distribution for $\beta\le 0.5$. At the largest value of Q^2 we are going to use the interpolation (68), namely $40\,\mathrm{GeV}^2$, and for $\beta\simeq 0.2$ it deviates less than 5% from the CTEQ gluon distribution. For values of β in the range 10^{-4}–10^{-1}, the interpolation (68) agrees with the CTEQ gluon distribution within 1%. In this region the Q^2 dependence of δ is approximately given by

$$\delta(Q^2) \,=\, 0.17+0.07\ln\left(Q^2/Q_0^2\right)-0.005\ln^2\left(Q^2/Q_0^2\right)\,. \tag{70}$$

The parameterization (68), (69) and (70) effectively takes into account the evolution of the gluon distribution in a large but finite range of Q^2 as calculated in [41]. At small β the gluon distribution has a typical error of about 15% [41]. Within this error there is agreement with the analysis presented in [42]. An error assessment of the power δ provides an uncertainty of about 10–15% for it [41,42].

For the various terms in the ansatz (68) the integrations occurring in (65) can be performed analytically [36]. One finds

$$\begin{aligned} H_{1i}(\bar{x},\xi) &= \frac{3}{2\xi^3}\,\frac{\Gamma(1+i/2-\delta)}{\Gamma(4+i/2-\delta)} \\ &\times\Big\{(\xi^2-\bar{x})\left[x_1^{2+i/2-\delta}-x_2^{2+i/2-\delta}\right] \\ &\quad+\xi(1-\bar{x})(2+i/2-\delta)\left[x_1^{2+i/2-\delta}+x_2^{2+i/2-\delta}\right]\Big\}\,, \\ &\quad \bar{x}\ge\xi\,, \\ &= \frac{3}{2\xi^3}\,\frac{\Gamma(1+i/2-\delta)}{\Gamma(4+i/2-\delta)} \\ &\times\Big\{x_1^{2+i/2-\delta}\left[\xi^2-\bar{x}+(2+i/2-\delta)\xi(1-\bar{x})\right] \\ &\quad+(\bar{x}\to-\bar{x})\Big\}\,, \\ &\quad \bar{x}\le\xi\,, \end{aligned} \tag{71}$$

for the case $n=1$. A similar but somewhat more complicated results are obtained for the case $n=2$.

This way we obtain an expansion of H^g

$$H^g(\bar{x},\xi) \,=\, \sum_i \hat{c}_{ni}\,H_{ni}(\bar{x},\xi)\,, \tag{72}$$

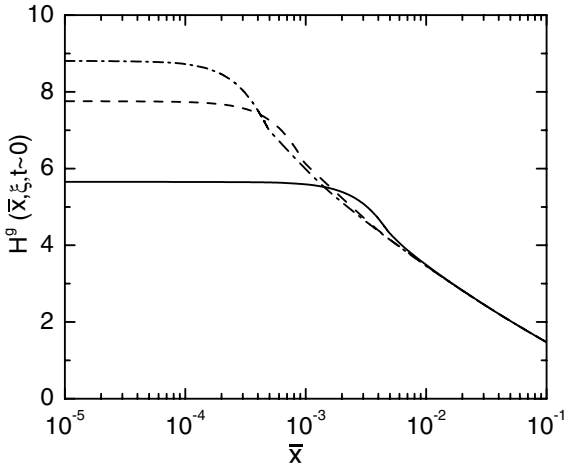

Fig. 3. Model results for the GPD H^g in the small $\bar{x}$ range at $t \simeq 0$ and for the case $n = 1$. The solid (dashed, dash-dotted) line represents the GPD at $\xi = 5\ (1\,,\ 0.5) \cdot 10^{-3}$ and at the scale 2 GeV

with coefficients following from (68). The evolution of the GPD is here approximated by that of the gluon distribution. The dominant contribution to vector-meson electroproduction comes from the imaginary part of the L → L amplitude (see Sect. 6) which is $\propto H^g(\xi,\xi)$. Since, to a good approximation, $H^g(\xi,\xi)$ equals $x_{\rm Bj}\, g(x_{\rm Bj})$ at small ξ we have approximately taken into account the evolution. The full evolution of the gluonic GPD is complicated because of mixing with the flavor-singlet quark GPD. Its modeling would counteract any possible gain of accuracy obtained by the inclusion of the full evolution behavior.

The GPD H^g and its derivatives up to order n are continuous at $\bar{x} = \xi$. For $\xi \ll \bar{x}$ one can convince oneself that $H^g(\bar{x},\xi) \to \bar{x}\, g(\bar{x})$ up to corrections of order ξ^2. In the forward limit, $\xi, t \to 0$, the GPD H^g reduces to the ordinary parton distribution $\bar{x}g(\bar{x})$. Results for H^g in the case $n = 1$ are shown in Fig. 3. For $\bar{x}$ larger than $\xi \ll 1$ there is practically no dependence on the skewness in contrast to the region $\bar{x} \le \xi$ in accord with the general behavior of the model GPD just mentioned. The GPDs for $n = 1$ and 2 agree with each other on the percent level at small $\bar{x}$. As we checked the numerical results for the cross sections obtained with both these GPDs are very similar; the differences in the imaginary (real) parts of the amplitudes are typically smaller than 1(7)%. In the following we will therefore show only numerical results for the case $n = 1$.

Considering the collinear limit of the subprocess amplitude (45), one notices a double pole $(\bar{x}-\xi+\mathrm{i}\varepsilon)^{-2}$ occurring in the T → T amplitude (24) [16]. Partial integration leads to the integral

$$\sim \int_0^1 \frac{\mathrm{d}\bar{x}}{\bar{x}-\xi+\mathrm{i}\varepsilon}\, \frac{\mathrm{d}}{\mathrm{d}\bar{x}} \left[H^g(\bar{x},\xi)\tilde{f}(\bar{x},\xi)\right], \qquad (73)$$

where $\tilde{f}$ arises from the subprocess amplitude (45). Since the derivatives of H^g and $\tilde{f}$ are continuous at $\bar{x} = \xi$ the integral exist. The transverse quark momenta are not needed for the regularization of the T → T amplitude.

A model for the GPD $\widetilde{H}^g$ can be constructed analogously to (63) and (65), the parton distribution $g(\beta)$ is only to be replaced by its polarized counterpart $\Delta g(\beta)$. The continuation to negative β is defined by

$$\Delta g(-\beta) \;=\; \Delta g(\beta)\,. \qquad (74)$$

The GPD $\widetilde{H}^g$ is antisymmetric in $\bar{x}$

$$\widetilde{H}^g(-\bar{x},\xi) = -\widetilde{H}^g(\bar{x},\xi)\,. \qquad (75)$$

We take Δg from [43] and parameterize it analogously to (68)

$$\beta\Delta g(\beta) \;=\; \beta^{\tilde{\delta}(Q^2)}\,(1-\beta)^5 \sum_{i=0}^{2} \tilde{c}_i\,\beta^i\,, \qquad (76)$$

where

$$\begin{aligned} \tilde{c}_0 &= 3.39 - 0.864\,\ln(Q^2/Q_0^2)\,, \qquad (77)\\ \tilde{c}_1 &= 1.73 + 0.24\,\ln(Q^2/Q_0^2) - 0.17\,\ln^2(Q^2/Q_0^2)\\ \tilde{c}_2 &= 0.42 - 0.115\,\ln(Q^2/Q_0^2) - 0.069\,\ln^2(Q^2/Q_0^2)\,, \end{aligned}$$

and

$$\tilde{\delta}(Q^2) \;=\; 0.78 - 0.173\,\ln(Q^2/Q_0^2)\,. \qquad (78)$$

The GPD $\widetilde{H}^q$ can than calculated analytically for either case, $n = 1$ and 2, with, for instance, the help of (71). It is then represented by a sum analogously to (72). We finally remark that the polarized gluon distribution and hence $\widetilde{H}^g$ is subject to much larger uncertainties than H^g.

6 Cross sections

Vector-meson electroproduction in the diffractive region has been extensively investigated at HERA [12–14,44–46] for large W and Q^2 but small $x_{\rm Bj}$. Preliminary data from H1 and ZEUS [47–49] extend the range of Q^2 for which electroproduction data are available. In order to confront the data with the theory developed in the preceding sections, one has either to extrapolate the data to $t \simeq 0$ or to take into account the t dependencies of the GPD and the subprocess amplitudes. The latter recipe is not straightforward. As we mentioned in Sect. 5 it is not easy to find a plausible parameterization for the t dependence of the GPD because factorization in t and $\bar{x}, \xi$ most likely does not hold [38,39]. We therefore use a variant of the first recipe and multiply the $t \simeq 0$ amplitudes (24) and (57) by the exponentials

$$\sim \exp\left[t\, B_i^V/2\right], \qquad (79)$$

with slope parameters B_i^V (i = LL, LT, TT for L → L, T → L, T → T transitions, respectively) adjusted to experiment. The ansatz (79) is in accord with the expected exponential behavior of the GPDs [37,50]. Differences in the slope parameters arise from the t dependence of the subprocess amplitudes.

In the one-photon exchange approximation the $ep \to epV$ cross section integrated over the azimuthal angle reads

$$\frac{\mathrm{d}^3\sigma(ep \to ep\rho)}{\mathrm{d}y\mathrm{d}Q^2\mathrm{d}t} = \frac{\alpha_{\rm elm}}{2\pi}\,\frac{1+(1-y)^2}{y\,Q^2}\,\left[\frac{\mathrm{d}\sigma_{\rm T}}{\mathrm{d}t}+\varepsilon\frac{\mathrm{d}\sigma_{\rm L}}{\mathrm{d}t}\right], \tag{80}$$

where high-energy, small $x_{\rm Bj}$ approximations have been applied to the phase space factor. Under the same kinematical conditions the ratio of longitudinal to transversal polarization of the virtual photon is given by

$$\varepsilon \simeq 2\frac{1-y}{1+(1-y)^2}\,, \tag{81}$$

where y is the fraction of longitudinal electron momentum carried by the photon:

$$y = \frac{q\cdot p}{k_e\cdot p} = \frac{W^2+Q^2}{s}\,. \tag{82}$$

Here, k_e is the momentum of the incident electron and $s = (k_e+p)^2$. The $\gamma^* p \to Vp$ partial cross sections in (80) for transversally and longitudinally polarized virtual photons are related to the amplitudes (57) by

$$\begin{aligned}\frac{\mathrm{d}\sigma_{\rm T}}{\mathrm{d}t} &= \frac{1}{16\pi W^2\,(W^2+Q^2)}\left[\left|\mathcal{M}^H_{++,++}\right|^2+\left|\mathcal{M}^H_{0+,++}\right|^2\right],\\ \frac{\mathrm{d}\sigma_{\rm L}}{\mathrm{d}t} &= \frac{1}{16\pi W^2\,(W^2+Q^2)}\left|\mathcal{M}^H_{0+,0+}\right|^2,\end{aligned} \tag{83}$$

where we made use of (27), (41) and (58). Terms of order $\langle\widetilde{H}^g\rangle^2$ have been neglected in the cross sections (83); there is no interference between the H^g and $\widetilde{H}^g$ contributions.

The differential cross section data for $ep \to epV$ exhibit a characteristic diffraction peak at small t. The slope of the diffraction peak is found to be nearly independent of W but is mildly varying with Q^2. Most of the differential cross section data for ρ and ϕ production are compatible with a single exponential within errors. The combined H1 and ZEUS data on the slopes in the range $4\,\mathrm{GeV}^2 \lesssim Q^2 \lesssim 40\,\mathrm{GeV}^2$ can be condensed into

$$B^V_{\rm LL} = 7.5\,\mathrm{GeV}^{-2} + 1.2\,\mathrm{GeV}^{-2}\ln\frac{3.0\,\mathrm{GeV}^2}{Q^2+m_V^2}\,. \tag{84}$$

This parameterization is in rather good agreement with experiment, keeping in mind that the experimental slopes are not always extracted from cross section data in the same range of t. Possible deviations from a single exponential behavior of the cross sections then lead to different slopes. We naturally assign the slope (84) to the dominant L $\to$ L transition amplitude. The slopes of the other amplitudes are not well determined as yet. A detailed analysis of the spin-density matrix elements presented in Sect. 7, seems to favor the choice $B^V_{\rm LT} = 2B^V_{\rm TT} = B^V_{\rm LL}$ slightly. These slope values lead to results from our GPD based approach in fair agreement with the HERA data. It is to be stressed that the magnitude of the transverse cross section is controlled by the product of parameters $(f_{V\,\rm T}/M_V)^2/B^V_{\rm TT}$ leaving aside the mild Q^2 dependence of the slope. The just described fit is based on the choice $M_V = m_V$ (see the remark subsequent to (34)). Taking a smaller value for M_V and a corresponding value for the decay constant, the slope $B^V_{\rm TT}$ can be closer to that one for the L $\to$ L amplitude. For instance, choosing $M_V = m_V/2$, one may use $B^V_{\rm TT} = B^V_{\rm LL}$ (for $f_{\rho\,\rm T} = 170\,\mathrm{MeV}$ and $f_{\phi\,\rm T} = 190\,\mathrm{MeV}$), and one obtains almost identical results for the cross sections.

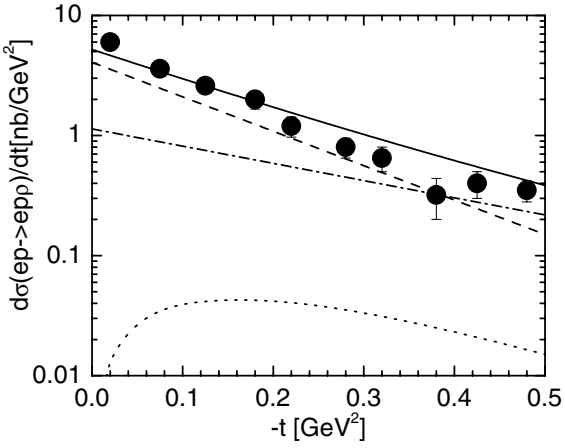

Fig. 4. The differential cross section (80) for $ep \to ep\rho$ versus $-t$ integrated over the kinematical region available to the ZEUS experiment from which the data are taken [13]. The solid line is our fit to the data at $W = 75\,\mathrm{GeV}$ and $Q^2 = 6\,\mathrm{GeV}^2$ (see text). The dashed (dot-dashed, short-dashed) line represents the individual contributions from the L $\to$ L (T $\to$ T, T $\to$ L) amplitudes

As a check of our choice of the slopes we show the ZEUS data [13] for the differential cross section of ρ production in Fig. 4. These data indicate deviations from a single exponential behavior. They are integrated over the W and Q^2 region accessible to ZEUS; W varies between 32 and 167 GeV in dependence on Q^2 which varies between 3 and $50\,\mathrm{GeV}^2$. The associated normalization uncertainty is of no bearing to us since we are interested in the process $\gamma^* p \to Vp$. The forward amplitudes (57) evaluated from the model GPD H^g shown in Fig. 3, multiplied with the exponentials (79), lead to the results for the $ep \to ep\rho$ differential cross section shown in Fig. 4. The agreement between our result and experiment is not too good. Obviously, the value of the slope taken from (84) at $Q^2 = 6\,\mathrm{GeV}^2$, is a bit too small. However, the data shown in Fig. 4, need confirmation. We can also see from the figure that our results, although obtained with different slopes, do not deviate from a single exponential behavior substantially. Also shown in Fig. 4 are the three individual contributions L $\to$ L, T $\to$ T and T $\to$ L separately. As expected the L $\to$ L contribution dominates. The T $\to$ T contributions amounts to about 25% of the L $\to$ L one at $t \simeq 0$. Due to the smaller slope $B^V_{\rm TT}$ takes the lead for $-t$ larger than about $0.4\,\mathrm{GeV}^2$. The T $\to$ L contribution is shown only for comparison, it is of no importance for the cross sections.

Let us now turn to the discussion of the process $\gamma^* p \to Vp$. The integrated cross section for this process is related

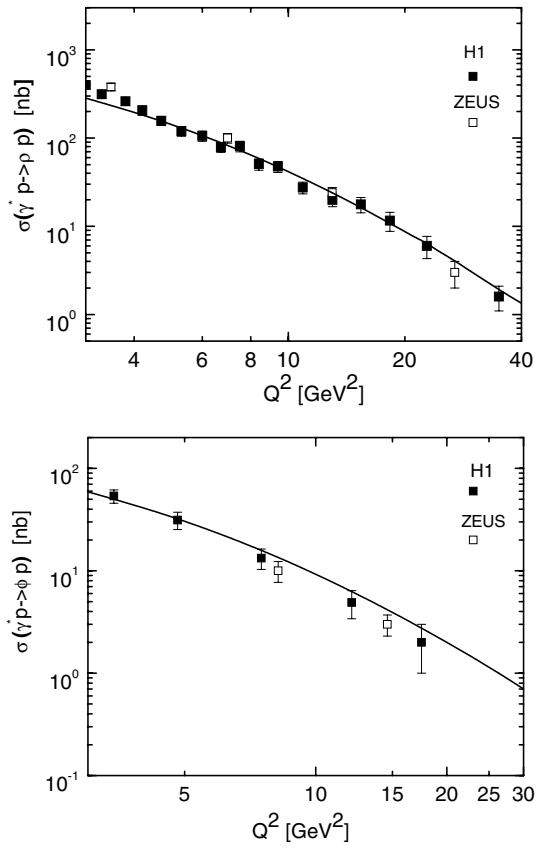

Fig. 5. The integrated cross section for $\gamma^* p \to \rho p$ (top) and $\gamma^* p \to \phi p$ (bottom) versus Q^2 at $W \simeq 75\,\mathrm{GeV}$. The data are taken from [12,44] (filled squares) and [13,45] (open squares) for ρ and ϕ production, respectively. The solid lines represent our results

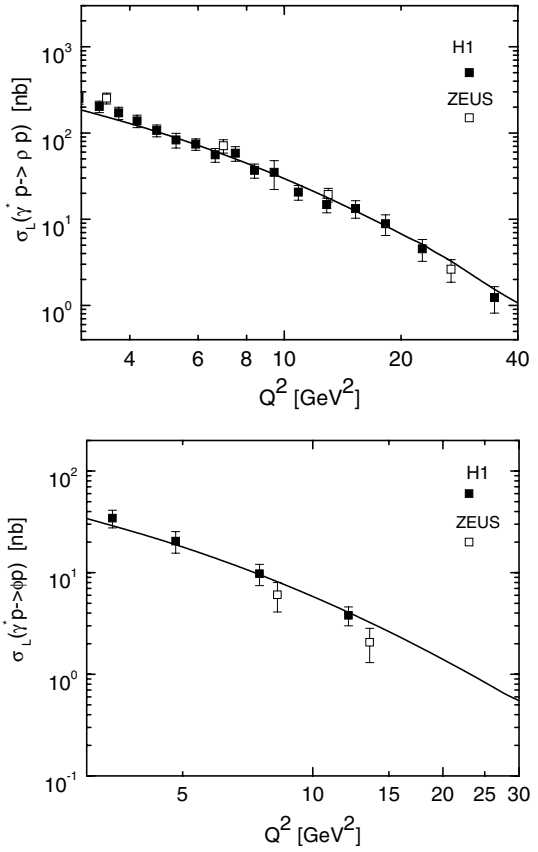

Fig. 6. The integrated cross section for longitudinally polarized photons versus Q^2 at $W \simeq 75\,\mathrm{GeV}$. Top: $\gamma_{\mathrm{L}}^* p \to \rho p$; bottom: $\gamma_{\mathrm{L}}^* p \to \phi p$. The data are taken from H1 [12,44,46] (filled squares) and ZEUS [13,45] (open squares), respectively. The solid lines represent our results

to the integrated partial cross sections (83) by

$$\sigma(\gamma^* p \to V p) \;=\; \sigma_{\mathrm{T}}(\gamma^* p \to V p) + \epsilon\, \sigma_{\mathrm{L}}(\gamma^* p \to V p)\,. \quad (85)$$

The H1 [12,44] and ZEUS [13,45] data on the cross sections for $\gamma^* p \to p V$ ($V = \rho, \phi$), integrated over the diffraction peak, are compared to our results in Fig. 5. We repeat that our results are evaluated from the handbag amplitude (57) multiplied by the exponentials (79) and using the GPD H^g shown in Fig. 3. Good agreement between model and experiment is achieved for both processes provided Q^2 is larger than about $4\,\mathrm{GeV}^2$.

The HERA experiments also measured the decay angular distributions of the ρ and ϕ mesons and determined their spin-density matrix elements. This information allows for a determination of the cross section ratio

$$R(V) \;=\; \frac{\sigma_{\mathrm{L}}(\gamma^* p \to V p)}{\sigma_{\mathrm{T}}(\gamma^* p \to V p)}\,, \quad (86)$$

from which, in combination with (85), the longitudinal cross section, σ_{L}, can be isolated as well. The HERA data for σ_{L} and R are compared to our results in Figs. 6 and 7, respectively. Again reasonable agreement is to be observed for Q^2 larger than $4\,\mathrm{GeV}^2$. The ratio R increases with Q^2 since the transverse cross section is suppressed by $1/Q^2$ as compared to the longitudinal one; see the hierarchy (41).

The experimental results on cross section ratio are derived from the data on the spin-density matrix element r_{00}^{04}. The extracted ratio is therefore the ratio of the differential cross sections (83):

$$\tilde{R}(V) \;=\; \frac{\mathrm{d}\sigma_{\mathrm{L}}(\gamma^* p \to V p)}{\mathrm{d}\sigma_{\mathrm{T}}(\gamma^* p \to V p)}\,, \quad (87)$$

which equals the ratio of integrated cross sections, R, only if both the differential cross sections show the same t dependence[6]. This is however not the case if the slopes differ. Therefore, $\tilde{R}$, measured at $t \simeq -0.15\,\mathrm{GeV}^2$, is about 10–20% larger than R. In Fig. 7 we also display our prediction for $\tilde{R}$. Very good agreement with experiment is to be seen now. It is to be stressed that the uncertainties of the gluon distribution [41] entail a typical error of about 30% for our predictions for the cross sections. In the ratios these errors cancel to some extent. As we remarked a fit

[6] For single exponentials the relation between R and $\tilde{R}$ is given by
$R = B_{\mathrm{TT}}/B_{\mathrm{LL}} \exp\left[-(B_{\mathrm{LL}} - B_{\mathrm{TT}})t\right] \tilde{R}(t)$.

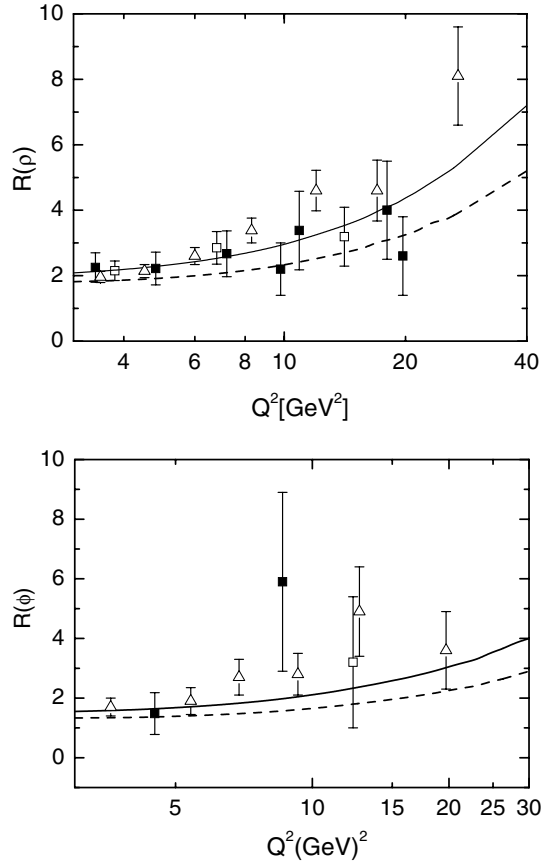

Fig. 7. The ratio of longitudinal and transverse cross sections for ρ (top) and ϕ (bottom) production versus Q^2 at $W \simeq 75\,\mathrm{GeV}$. The data are taken from [12,44,46] (filled squares) and [13,45] (open squares) for ρ and ϕ production, respectively. The open triangles represent preliminary ZEUS data [48,49] for ρ and ϕ electroproduction. The solid (dashed) lines are our results for the ratio of differential (integrated) cross sections, $\tilde{R}\,(R)$. The ratio $\tilde{R}$ is evaluated at $t = -0.15\,\mathrm{GeV}^2$

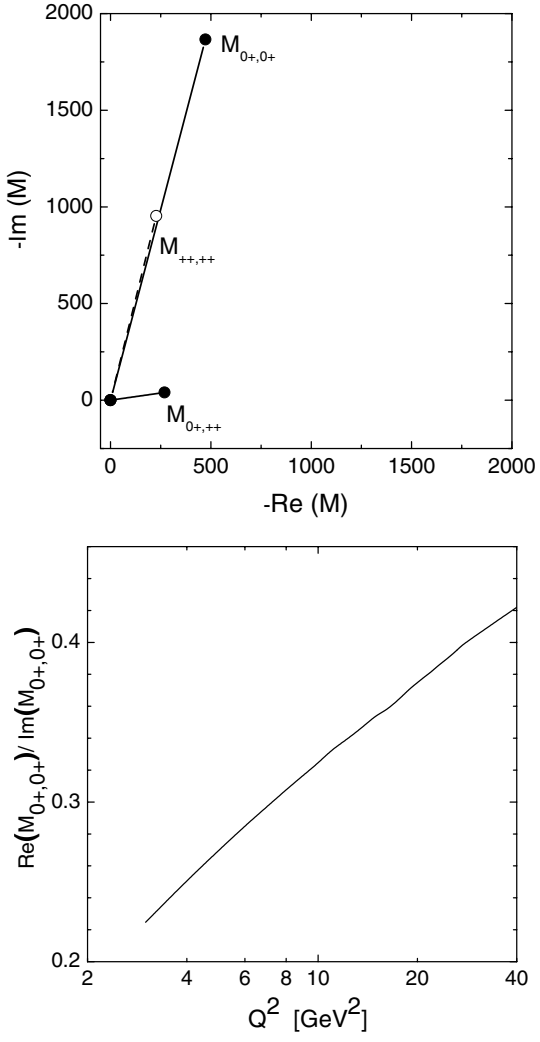

Fig. 8. Top: The ρ production amplitudes for the three transitions L $\to$ L, T $\to$ T and T $\to$ L at $Q^2 = 4\,\mathrm{GeV}^2$, $t = -0.15\,\mathrm{GeV}^2$ and $W = 75\,\mathrm{GeV}$. Bottom: Real over imaginary part of the amplitude $\mathcal{M}^H_{0+,0+}$ for ρ production versus Q^2 at $t \simeq 0$ and $W = 75\,\mathrm{GeV}$

with $B^V_{\mathrm{TT}} \simeq B^V_{\mathrm{LL}}$ is also in agreement with the present data provided the value of the product $(f_{V\,\mathrm{T}}/M_V)^2/B^V_{\mathrm{TT}}$ is kept constant. The ratio R for this fit practically falls together with $\tilde{R}$ in the fit presented above.

In Fig. 8 we display an Argand diagram of the three forward amplitudes for ρ electroproduction at $Q^2 = 4\,\mathrm{GeV}^2$, $t = -0.15\,\mathrm{GeV}^2$ and $W = 75\,\mathrm{GeV}$. Both $\mathcal{M}^H_{0+,0+}$ and $\mathcal{M}^H_{++,++}$ are dominantly imaginary while the T $\to$ L one is nearly real. The latter phase is a consequence of the branch point of $\sqrt{\bar{x}^2 - \xi^2}$ in (44). The hierarchy (41) is here seen again. The phase of the ρ production amplitude $\mathcal{M}^H_{0+,0+}$ at $t \simeq 0$ is shown in more detail on the top part of Fig. 8. The real over imaginary part ratio increases with Q^2 and takes values between 0.2 and 0.4 in the Q^2 region of interest. The real part of the L $\to$ L amplitude therefore contributes only about 10% to the cross sections.

A number of comments concerning the leading-twist contribution [9,11] are in order. As we mentioned above it is given by the collinear approximation of the dominant amplitude $\mathcal{M}^H_{0+,0+}$. The salient features of the leading-twist contribution are passed on to the full L $\to$ L amplitude, the quark transverse momenta and Sudakov suppressions essentially affect its absolute value. The examination of the leading-twist contribution therefore elucidates many properties of our results in a simple way. Neglecting the $k_\perp$ terms in (43) and using the standard definition of the meson distribution amplitude

$$\frac{f_{V\mathrm{L}}}{2\sqrt{2N_c}}\,\Phi_{V\mathrm{L}}(\tau) \;=\; \int \frac{\mathrm{d}^3\mathbf{k}_\perp}{16\pi^3}\,\Psi_{V\mathrm{L}}(\tau, k_\perp^2)\,, \qquad (88)$$

we obtain the subprocess amplitude $\mathcal{H}^V_{0+,0+}$ in collinear approximation from (42) and, inserting it into (24), the leading-twist contribution to the L $\to$ L amplitude

$$\mathcal{M}^{\mathrm{coll}}_{0+,0+} \qquad (89)$$
$$= e\,\frac{8\pi\alpha_{\mathrm{s}} f_{V\mathrm{L}}}{N_c Q}\,\langle 1/\tau\rangle_{V\mathrm{L}}\,\mathcal{C}_V \int_0^1 \mathrm{d}\bar{x}\,\frac{H^g(\bar{x},\xi)}{(\bar{x}+\xi)(\bar{x}-\xi+\mathrm{i}\hat{\varepsilon})}\,.$$

The $1/\tau$ moment of the meson's distribution amplitude $\Phi_{V\mathrm{L}}$ occurring now, is denoted by $\langle 1/\tau\rangle_{V\mathrm{L}}$. For the wave-function (47) the associated distribution amplitude is the asymptotic form (48) which leads to a value of 3 for the $1/\tau$ moment.

We can now easily understand the growth of the real over imaginary part ratio with Q^2. Applying the derivative analyticity relation [51], frequently but unjustifiedly termed the local dispersion relation [52], to the imaginary part of the leading-twist amplitude (89),

$$\mathcal{M}^{\mathrm{coll}}_{0+,0+} \simeq \left[\mathrm{i} - \frac{\pi}{2}\frac{\partial}{\partial \ln x_{\mathrm{Bj}}} x_{\mathrm{Bj}}\right] \mathrm{Im}\, \mathcal{M}^{\mathrm{coll}}_{0+,0+}\,, \qquad (90)$$

and using the low-ξ behavior of the model GPD $H^g(\xi,\xi) = \bar{c}_0(2\xi)^{-\delta}$ (see (71)), we find

$$\mathrm{Re}M^{\mathrm{coll}}_{0+,0+}/\,\mathrm{Im}M^{\mathrm{coll}}_{0+,0+} \simeq \frac{1}{2}\pi\,\delta(Q^2)\,. \qquad (91)$$

The increase of δ with Q^2 (see (70)) which has been calculated by the CTEQ group [41] with the help of QCD evolution, is what we see at the top part of Fig. 8.

Up to corrections from the real part the integrated longitudinal cross section reads

$$\sigma^{\mathrm{coll}}_{\mathrm{L}} = \frac{16\,\pi^4}{N_c^2}\,\frac{\alpha_{\mathrm{elm}}}{B^V_{\mathrm{LL}}\,Q^6}\left[\alpha_{\mathrm{s}}\, f_{V\mathrm{L}}\mathcal{C}_V\,\langle 1/\tau\rangle_{V\mathrm{L}}\right]^2 \left|H^g(\xi,\xi)\right|^2\,, \qquad (92)$$

in collinear approximation. The ratio of the ϕ and ρ cross sections is given by $(f_{\phi\mathrm{L}}\mathcal{C}_\phi/f_{\rho\mathrm{L}}\mathcal{C}_\rho)^2$. Our results shown in Figs. 5 and 6, approach this value with increasing Q^2. Due to the behavior of $H^g(\xi,\xi)$ at small ξ the cross section behaves as

$$\sigma^{\mathrm{coll}}_{\mathrm{L}} \propto W^{\,4\delta(Q^2)}\,, \qquad (93)$$

at fixed Q^2 and small x_{Bj}. The power behavior (93) comes about as a consequence of the behavior of the GPD and the underlying gluon distribution. We note in passing that in the Regge picture [2] the exponent $\delta(Q^2)$ is associated with pomeron exchange. The intercept of the pomeron trajectory is related to δ by $\alpha_P(0) = 1 + \delta(Q^2)$. In the Regge model δ is a free parameter.

In Fig. 9 we display the cross section for $\gamma^* p \to \rho p$ as a function of W for sample values of Q^2. Fair agreement between experiment and our predictions is to be seen. The W dependence of the predictions from the full approach is very close to that given in (93). Deviations from the power law at lower values of W, to be observed in Fig. 9, arise from various corrections to the leading-twist contribution we take into account, such as the quark transverse momenta, the T $\to$ T amplitude and the real parts of the L $\to$ L amplitude. This interpretation of the power behavior of σ_{L} is supported by a comparison of δ as taken from the analysis presented in [41], with the powers obtained from fits to the cross section data [12,13]. Rough agreement between both results is to be seen in Fig. 9, although the errors of the HERA data do not permit a definite conclusion as yet. Preliminary HERA data seem to improve the agreement.

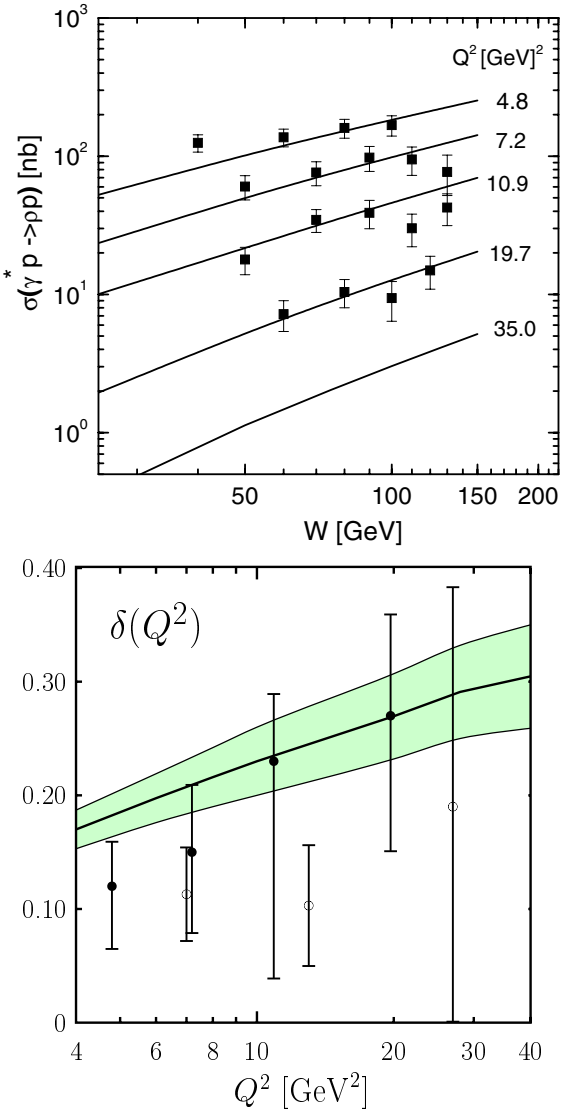

Fig. 9. Top: The integrated cross section for $\gamma^* p \to \rho p$ versus W for five values of Q^2. The data are taken from [12]. The solid lines represent our result. Bottom: The power δ versus Q^2 for ρ electroproduction. The solid curve represents the power as determined in [41] with an error estimate given by the shaded band. The data are taken from [12] (•) and [13] (∘)

For very small ξ one can estimate the size of the collinear contribution using the leading terms in the model GPD (71). One obtains

$$\begin{aligned}\sigma^{\mathrm{coll}}_{\mathrm{L}}&(\gamma^* p \to \rho p)\\ &= 5.72\,\mu\mathrm{b\,GeV}^6\left(\frac{\alpha_{\mathrm{s}}}{0.3}\right)^2\left(\frac{7.5\,\mathrm{GeV}^{-2}}{B^\rho_{\mathrm{LL}}}\right)\left(\frac{\bar{c}_0(Q^2)}{2.33}\right)^2\\ &\quad\times\left(\frac{\langle 1/\tau\rangle_{\rho\mathrm{L}}}{3}\right)^2\frac{(2\xi)^{-2\delta(Q^2)}}{Q^6}\,, \qquad (94)\end{aligned}$$

where $\bar{c}_0 = c_0/[(1-\delta/3)(1-\delta/2)]$ is the coefficient of the first term in the power series of H^g (72) associated with

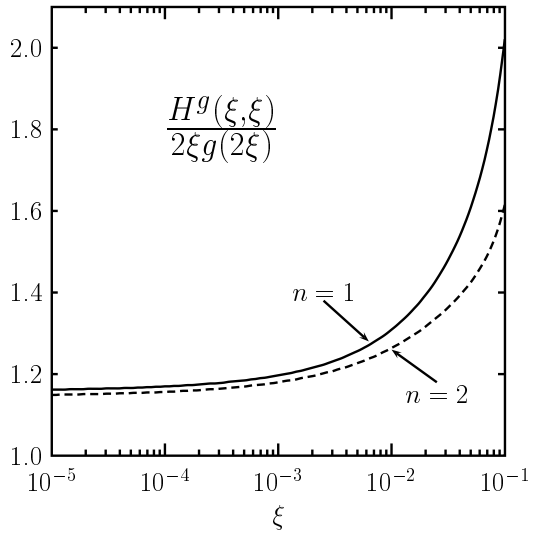

Fig. 10. Ratios of the GPDs and the parton distribution for the $n = 1$ and 2 models at a scale of $4\,\mathrm{GeV}^2$

(68). This cross section is rather large, well above experiment. The quark transverse momenta and the Sudakov factor suppress it such that agreement with experiment is found; see Fig. 6.

Exploiting the leading $\ln(1/x_{\rm Bj})$ approximation, Brodsky et al. [4] found a result[7] that equals (92) except that $H^g(\xi,\xi)$ is replaced by the usual gluon distribution $x_{\rm Bj}g(x_{\rm Bj})$ (see also [53]). At very small ξ, i.e. if ξ is so small that the first terms in (68) and in the corresponding GPD (72) suffice, the usual gluon distribution and the GPD only differ by about 20% resulting from the difference between c_0 and $\bar{c}_0$. For larger ξ, however, the difference between both functions becomes substantial, growing up to about a factor of 1.6–2 at $\xi = 0.1$; see Fig. 10. The use of the $\ln(1/x_{\rm Bj})$ approximation at values of ξ around 0.1 may therefore lead to an underestimate of the gluonic contribution to the cross sections by a factor 3 to 4. We repeat that, in contrast to the $\ln(1/x_{\rm Bj})$ approximation, we do not require a small ξ in principle. We only restrict ourselves to small ξ in order to avoid complications with potential contributions from quarks emitted and reabsorbed by the proton. The enhancement effect apparent in Fig. 10 is known as the skewing effect and has been discussed by several authors [8,15,54,55]. The size of the skewing effect estimated in these papers is compatible with our model result for $\xi \ll 1$.

In any case the leading-twist as well as the $\ln(1/x_{\rm Bj})$ result provide cross sections that are too large. In order to settle this problem for the $\ln(1/x_{\rm Bj})$ approximation Frankfurt et al. [6] estimated a correction factor by allowing for quark transverse momenta in the loop. This mechanism bears resemblance to our approach as we mentioned in Sect. 3. The correction factor obtained in [6] is large enough to achieve agreement with experiment. This factor has also been used by Mankiewicz et al. [15] in an explorative study of $\sigma_{\rm L}$ in an otherwise collinear GPD approach. Martin et al. [8] exploited the $\ln(1/x_{\rm Bj})$ approximation in their analysis of vector-meson electroproduction by including parton transverse momenta and an unintegrated gluon distribution.

[7] Note that in [4] the decay constant includes the flavor weight factor $\mathcal{C}_V$.

7 Spin density matrix elements

With the help of (27), (41) and (58) the spin-density matrix elements extracted from the decay angular distributions measured with unpolarized leptons and protons [34], simplify to ($\tilde{R}$ is defined in (87))

$$
\begin{aligned}
N_{\rm L} &= 2\left|\,\mathcal{M}^H_{0+,0+}\right|^2,\\
N_{\rm T} &= 2\left[\,\left|\mathcal{M}^H_{++,++}\right|^2+\left|\mathcal{M}^H_{0+,++}\right|^2\right],\\
r^{04}_{00} &= \frac{1}{1+\varepsilon\tilde{R}}\left[\frac{2}{N_{\rm T}}\left|\mathcal{M}^H_{0+,++}\right|^2+\varepsilon\tilde{R}\right],\\
\mathrm{Re}\, r^{04}_{10} &= -\mathrm{Re}\, r^1_{10} \;=\; \mathrm{Im}\, r^2_{10}\\
&= \frac{1}{1+\epsilon\tilde{R}}\,\frac{1}{N_{\rm T}}\,\mathrm{Re}\,\left[\,\mathcal{M}^H_{++,++}\,\mathcal{M}^{H*}_{0+,++}\right],\\
r^1_{00} &= \frac{-1}{1+\epsilon\tilde{R}}\,\frac{2}{N_{\rm T}}\left|\mathcal{M}^H_{0+,++}\right|^2,\\
r^1_{1-1} &= -\mathrm{Im}\, r^2_{1-1}\\
&= \frac{1}{1+\epsilon\tilde{R}}\,\frac{1}{N_{\rm T}}\left|\mathcal{M}^H_{++,++}\right|^2,\\
r^5_{00} &= \frac{4}{\sqrt{2N_{\rm L}\,N_{\rm T}}}\,\frac{\sqrt{\tilde{R}}}{1+\epsilon\tilde{R}}\,\mathrm{Re}\,\left[\,\mathcal{M}^H_{0+,0+}\,\mathcal{M}^{H*}_{0+,++}\right],\\
\mathrm{Re}\, r^5_{10} &= -\mathrm{Im}\, r^6_{10}\\
&= \frac{\sqrt{\tilde{R}}}{1+\epsilon\tilde{R}}\,\frac{1}{\sqrt{2N_{\rm L}\,N_{\rm T}}}\,\mathrm{Re}\,\left[\,\mathcal{M}^H_{++,++}\,\mathcal{M}^{H*}_{0+,0+}\right],
\end{aligned}
\qquad (95)
$$

while

$$
r^{04}_{1-1} = r^1_{11} = r^5_{11} = r^5_{1-1} = \mathrm{Im}\, r^6_{1-1} = 0\,, \qquad (96)
$$

because of the neglect of $\mathrm{L}\to\mathrm{T}$ and $\mathrm{T}\to-\mathrm{T}$ transitions. The relations (95), obtained in the GPD approach under the assumption of the dominance of the H^g terms, coincide with those found assuming dominance of natural parity t-channel exchanges and the neglect of proton helicity flip [12,34]. The contributions from $\widetilde{H}^g$ enter the spin-density matrix elements only as bilinears; there are no interferences between H^g and $\widetilde{H}^g$ terms.

The data for the spin-density matrix elements from H1 [12,44] and ZEUS [14] are shown in Figs. 11 and 12 and compared to the results from the GPD based approach. The general pattern of the data is reproduced. The dominance of the $\mathrm{L}\to\mathrm{L}$ transition amplitude is clearly visible in the angular distribution of the production and decay of the vector mesons, in particular in the value of r^{04}_{00} which tends towards 1 with increasing Q^2. This behavior is well reproduced by our approach as we already discussed in connection with the cross section ratio R.

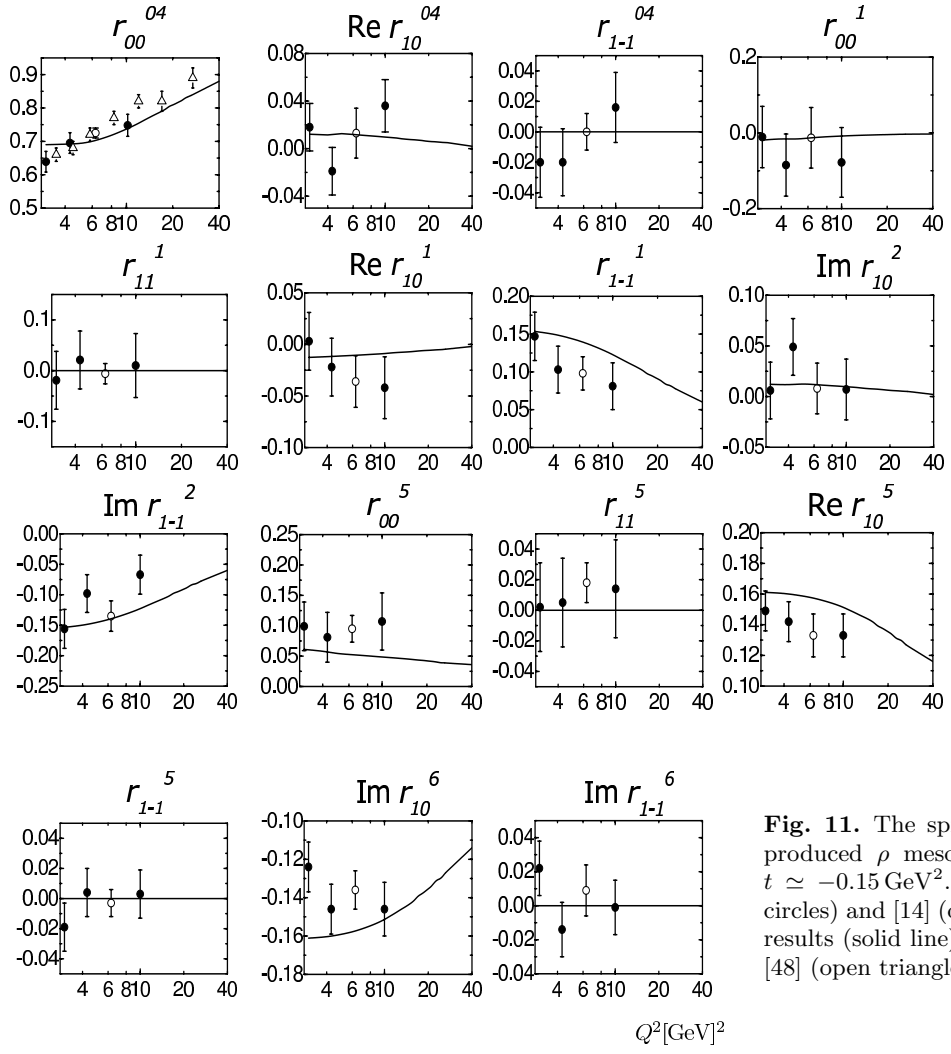

Fig. 11. The spin-density matrix elements of electroproduced ρ mesons versus Q^2 at $W \simeq 75\,\mathrm{GeV}$ and $t \simeq -0.15\,\mathrm{GeV}^2$. The data are taken from [12] (filled circles) and [14] (open circles); they are compared to our results (solid line). Preliminary data on r_{00}^{04} from ZEUS [48] (open triangles) are also shown

The T $\to$ L amplitude is probed by the matrix elements r_{00}^1 and r_{00}^5. While the first matrix element is approximately $\propto |\mathcal{M}^H_{0+,++}|^2/|\mathcal{M}^H_{0+,0+}|^2$, the ratio $\mathrm{Im}\,\mathcal{M}^H_{0+,++}/\mathrm{Im}\,\mathcal{M}^H_{0+,0+}$ essentially controls the second. Both r_{00}^5 and $|r_{00}^1|$ are found to be rather small. The ratio of the T $\to$ T and L $\to$ L amplitudes is approximately measured by r_{1-1}^1 and Re r_{10}^5, quadratically in the first case; linearly in the second one since the two amplitudes have about the same phase as is shown in Fig. 8. The fair agreement between theory and experiment for these spin-density matrix elements tells us that our approach provides the correct sizes and relative phases of the T $\to$ T and L $\to$ L amplitudes. The matrix elements $\mathrm{Re}\, r_{10}^{04} = -\mathrm{Re}\, r_{10}^1 = \mathrm{Im}\, r_{10}^2$ measure an interference term between the T $\to$ T and T $\to$ L amplitudes which is very small. Also this prediction is in acceptable agreement with experiment.

The t dependence of the spin-density matrix elements confirms the above observations; see Fig. 13. The T $\to$ L sensitive matrix elements behave proportional to $\sqrt{-t}$ or t while those controlled by the ratios of the T $\to$ T and L $\to$ L amplitudes exhibit an t dependence according to the different slopes chosen for them. As we mentioned in Sect. 6 the freedom in choosing a suitable value of M_V also allows for fits with $B^V_{\mathrm{TT}} \simeq B^V_{\mathrm{LL}}$. While the transverse cross section is nearly insensitive to this choice provided the product $(f_{V\,\mathrm{T}}/M_V)^2/B^V_{\mathrm{TT}}$ is approximately kept fixed, the t dependence of some of the spin-density matrix elements (e.g. r_{00}^{04}, r_{1-1}^1) changes; they become very flat in t. Given the accuracy of the present data [12] such a behavior is not in conflict with experiment.

Finally, in Fig. 14 we show our predictions for ϕ electroproduction at $W = 10\,\mathrm{GeV}$ characteristic of the COMPASS experiment.

Other theoretical analyses [7, 56–58] of the spin-density matrix elements are based on variants of the $\ln(1/x_{\mathrm{Bj}})$ approximation. The variants differ from each other in the detailed treatment of the subprocess $\gamma^* g \to q\bar{q}g$. The same hierarchy of the amplitudes are obtained as we find and, in general, rather similar results are obtained for the spin-density matrix elements. Worth mentioning is the different phase of the T $\to$ L amplitude and a somewhat different t dependence of the matrix elements.

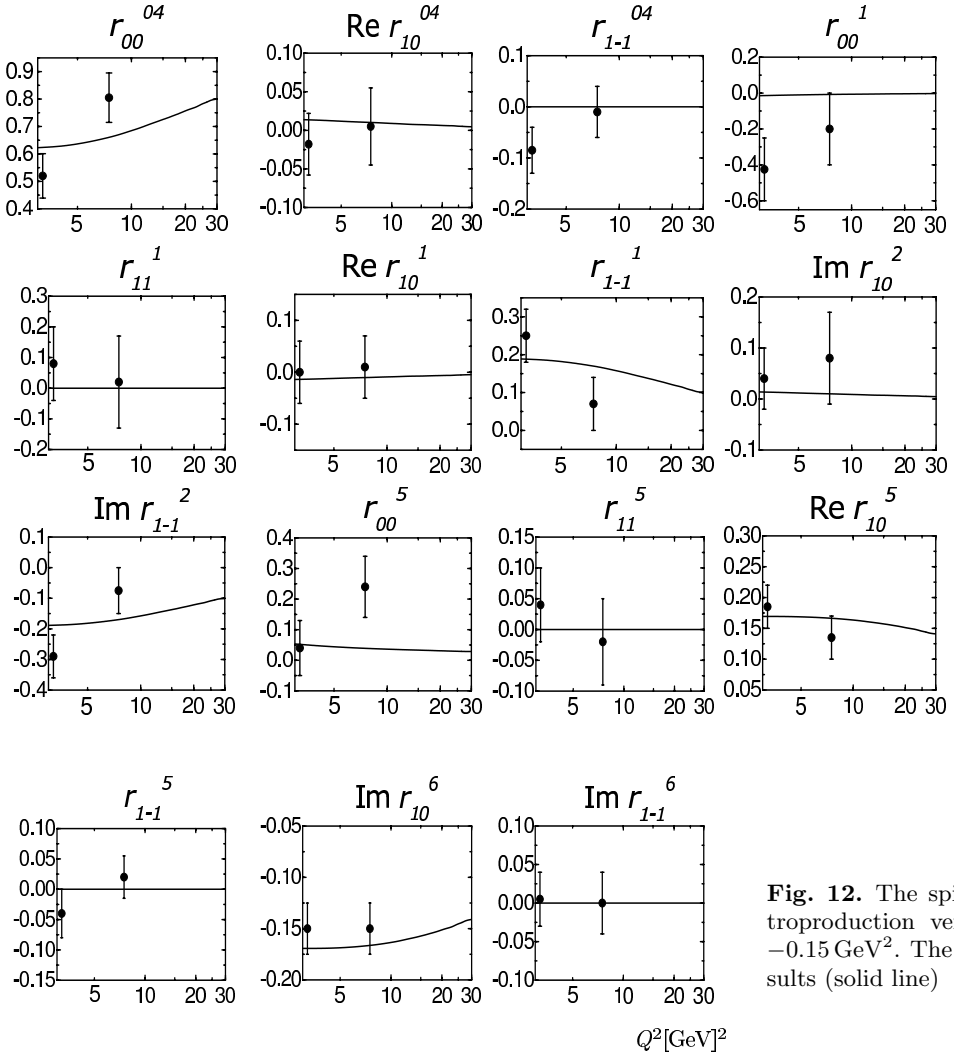

Fig. 12. The spin-density matrix elements for ϕ electroproduction versus Q^2 at $W \simeq 75\,\mathrm{GeV}$ and $t \simeq -0.15\,\mathrm{GeV}^2$. The H1 data [44] are compared to our results (solid line)

8 The helicity correlation

Finally, we want to discuss the role of the GPD $\widetilde{H}^g$. For this purpose we consider the initial state helicity correlation A_{LL} which can be measured with longitudinally polarized beam and target. After integration over the azimuthal angle this correlation reads

$$A_{\mathrm{LL}}[ep \to epV] = \frac{\sqrt{1-\varepsilon^2}}{32\pi W^2(W^2+Q^2)} \times \frac{\left|\mathcal{M}_{++,++}\right|^2 + \left|\mathcal{M}_{0+,++}\right|^2 - \left|\mathcal{M}_{-+,-+}\right|^2 - \left|\mathcal{M}_{0+,-+}\right|^2}{\mathrm{d}\sigma_{\mathrm{T}}/\mathrm{d}t + \varepsilon \mathrm{d}\sigma_{\mathrm{L}}/\mathrm{d}t}\,, \tag{97}$$

where the amplitudes and cross sections refer to the process $\gamma^* p \to Vp$ and are given in (24) and (83). As can easily be seen from (58) $A_{\mathrm{LL}} = 0$ if the $\widetilde{H}^g$ terms are neglected as we did in the preceding sections. Yet in contrast to the cross sections and spin-density matrix elements where the corrections are bilinear in the $\widetilde{H}^g$ terms and, hence, extremely small, the leading term in A_{LL} is an interference between the H^g and the $\widetilde{H}^g$ terms. In fact, with the help of (27) and (58), one obtains from (97)

$$A_{\mathrm{LL}}[ep \to epV] \;=\; 2\sqrt{1-\varepsilon^2}\,\frac{\mathrm{Re}\,\left[\mathcal{M}^{H}_{++,++}\,\mathcal{M}^{\widetilde{H}*}_{++,++}\right]}{\varepsilon|\mathcal{M}^{H}_{0+,0+}|^2 + |\mathcal{M}^{H}_{++,++}|^2}\,. \tag{98}$$

Obviously, this ratio is of order $\langle k_\perp^2\rangle/Q^2\ \langle\widetilde{H}^g\rangle/\langle H^g\rangle$ and, therefore, very small values for A_{LL} are to be expected. Indeed exploiting the model GPDs presented in Sect. 5 we confirm this assertion as can be seen from Fig. 15 where results for A_{LL} for ρ and ϕ electroproduction at $t \simeq 0$ are displayed. The results for ρ production, only shown at $W = 15\,\mathrm{GeV}$, are compared to the SMC data [59]. At this energy and in the range of Q^2 shown in the plot, the contribution from the quark GPD is expected to be small [17]. Our results for A_{LL} are not in disagreement with experiment given the admittedly large experimental errors and the rather large value of the skewness. Results for ϕ electroproduction are shown at energies typical for the HERMES and COMPASS experiments. The dominance of the gluon over the sea quarks permits this. At $W = 5\,\mathrm{GeV}$ A_{LL} is not very small since the major contribution to it

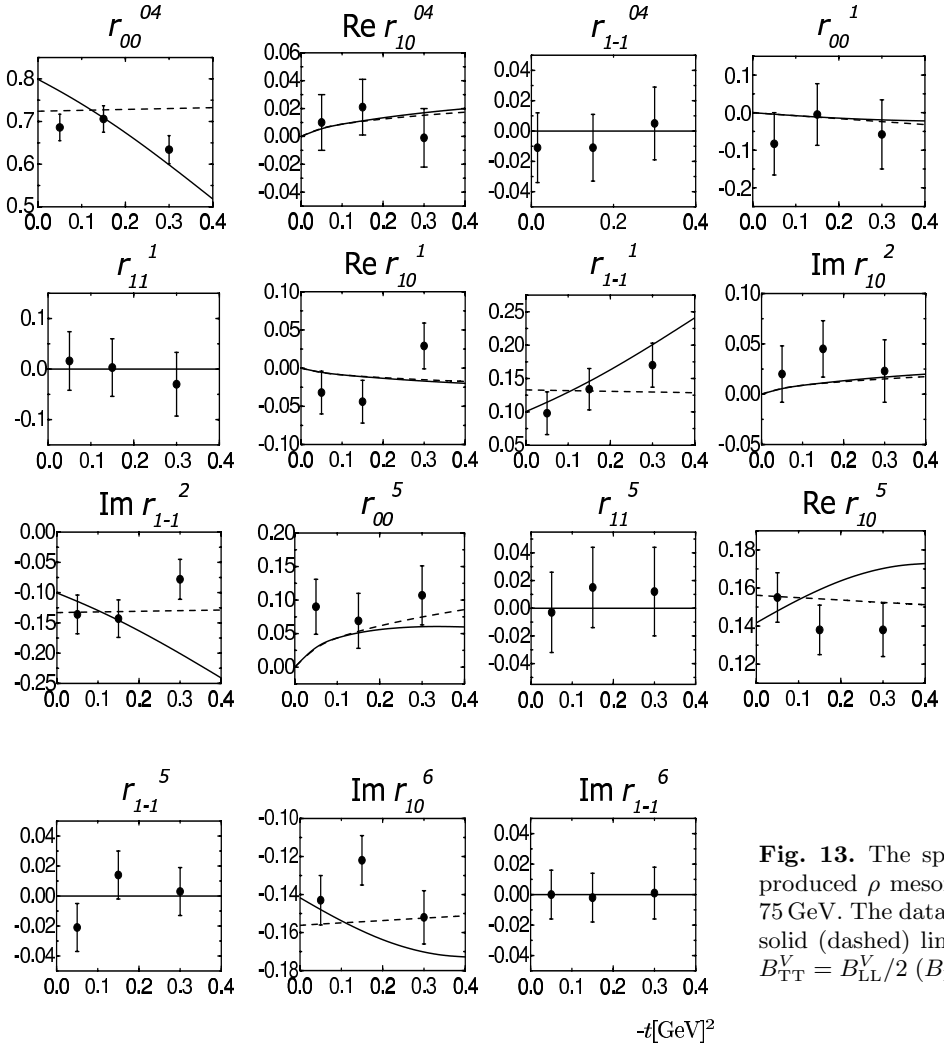

Fig. 13. The spin-density matrix elements of electroproduced ρ mesons versus t at $Q^2 = 5\,\mathrm{GeV}^2$ and $W \simeq 75\,\mathrm{GeV}$. The data are taken from [12] (filled circles). The solid (dashed) lines represent our results for the choice $B^V_{\mathrm{TT}} = B^V_{\mathrm{LL}}/2$ (B^V_{LL})

comes from the region $0.1 \lesssim \bar{x} \lesssim 0.2$ where $\Delta g/g$ is not small.

The proton helicity flip contribution, related to the GPD E^g, may change these results but likely not substantially. The helicity correlation will increase with growing momentum transfer if the slope of the T $\to$ T amplitude is smaller than that of the L $\to$ L one. Besides allowing for predictions for A_{LL} this calculation also supports our assumption of negligible contributions from $\widetilde{H}^g$ to the cross sections and spin-density matrix elements.

9 Summary

We analyzed electroproduction of light vector mesons at small x_{Bj} within a GPD based approach. In this kinematical domain the gluonic GPD H^g, parameterizing the response of the proton to the emission and reabsorption of gluons, controls the process. The gluonic GPD, not calculable at present, is constructed from an ansatz for the double distributions currently in use. In order to examine the influence of the model GPD on the numerical results for vector-meson electroproduction we used two different versions for it ($n = 1$ and 2). The differences in the numerical results obtained from these two models are on the percent level. The subprocess amplitudes for $\gamma^* g \to Vg$ are calculated by us to lowest order of perturbative QCD but transverse momenta of the quark and antiquark that form the vector meson are taken into account as well as Sudakov suppression, which sums up gluonic radiative corrections.

The GPD approach reproduces all main features of vector-meson electroproduction at small x_{Bj} known from phenomenology. The dominance of the contributions from the GPD H^g over those from $\widetilde{H}^g$ and E^g leads to the relations (58) and, hence, to results equivalent to those obtained assuming the dominance of natural parity exchange. Approximate s-channel helicity conservation holds due to the hierarchy (41) the amplitudes respect in our GPD based approach. The behavior of the longitudinal cross section as a Q^2 dependent power of W at fixed Q^2 is a consequence of the low ξ properties of the GPD and QCD evolution. The numerical results we obtain from our approach are in reasonable agreement with the small x_{Bj} data on cross sections and spin-density matrix elements

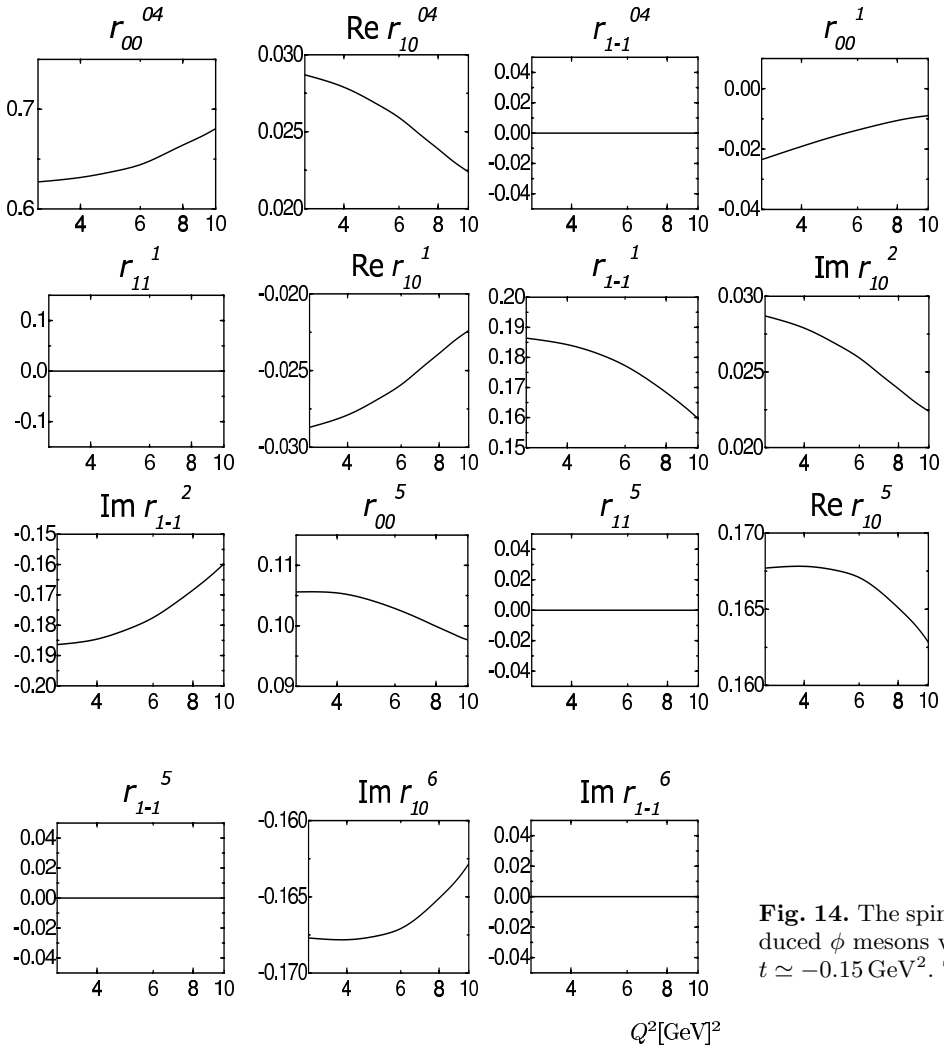

Fig. 14. The spin-density matrix elements of electroproduced ϕ mesons versus Q^2 at $W \simeq 10\,\mathrm{GeV}$, $y \simeq 0.6$ and $t \simeq -0.15\,\mathrm{GeV}^2$. The solid lines represent our results

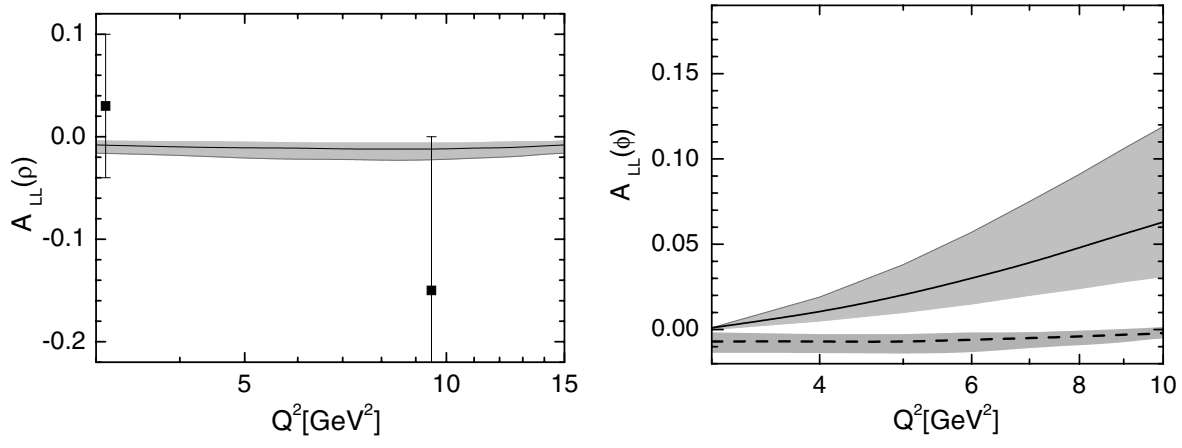

Fig. 15. Left: The helicity correlation A_{LL} for ρ electroproduction versus Q^2 at $W = 15\,\mathrm{GeV}$, $t \simeq 0$ and $y \simeq 0.6$. The data are taken from SMC [59]. Right: A_{LL} for ϕ production at $W = 5\,\mathrm{GeV}$ (solid line) and $W = 10\,\mathrm{GeV}$ (dashed line); $y \simeq 0.6$. The shaded bands reflect the uncertainties in our predictions due to the error in the polarized gluon distribution [43]

for electroproduction of ρ and ϕ mesons measured by H1 and ZEUS. The t dependence of vector-meson electroproduction is not yet satisfactorily settled. In principle it is generated by a combination of the t dependence of the GPD and, with less importance, that of the subprocess amplitudes. Due to the lack of a plausible parameterization of the t dependence of the GPD we have evaluated the electroproduction amplitudes at $t \simeq 0$ and multiplied them by exponentials in t. Improvements on this recipe are demanded and will be unavoidable as soon as detailed differential cross section data are at hand.

We also compared in some detail our approach to the leading-twist contribution and to the leading $\ln(1/x_{\rm Bj})$ approximation. The latter is rather close to the GPD approach at low $x_{\rm Bj}$ and small t but not identical. For $x_{\rm Bj}$ larger than about 0.01 the replacement of $H^g(\xi,\xi)$ by $2\xi g(2\xi)$ becomes inappropriate. The GPD has, in contrast to the leading $\ln(1/x_{\rm Bj})$ approximation, the potential to investigate the t dependence of electroproduction. The lack of understanding of the GPD's t dependence prevents this at present.

Acknowledgements. We thank A. Borissov, A. Efremov, O. Nachtmann, H. Meyer, E. Paul, A. Sandacz and L. Szymanowski for discussions and A. Bruni for providing us with preliminary ZEUS data. This work has been supported in part by the Russian Foundation for Basic Research, Grant 03-02-16816, the Integrated Infrastructure Initiative "Hadron Physics" of the European Union, contract No. 506078 and by the Heisenberg–Landau program.

References

1. D. Schildknecht, G.A. Schuler, B. Surrow, Phys. Lett. B **449**, 328 (1999)
2. A. Donnachie, P.V. Landshoff, Phys. Lett. B **437**, 408 (1998); J. Bartels, H. Kowalski, Eur. Phys. J. C **19**, 693 (2001); hep-ph/0010345
3. A. Donnachie, P.V. Landshoff, Phys. Lett. B **185**, 403 (1987);
   O. Nachtmann, contribution to the Ringberg workshop on HERA physics 2003; hep-ph/0312279
4. S.J. Brodsky, L. Frankfurt, J.F. Gunion, A.H. Mueller, M. Strikman, Phys. Rev. D **50**, 3134 (1994) [hep-ph/9402283]
5. B.Z. Kopeliovich et al., Phys. Lett. B **309**, 179 (1993); J. Nemchik et al., Z. Phys. C **75**, 71 (1997); I. Royen, J.R. Cudell, Nucl. Phys. B **545**, 505 (1999)
6. L. Frankfurt, W. Koepf, M. Strikman, Phys. Rev. D **54**, 3194 (1996) [hep-ph/9509311]
7. D.Y. Ivanov, R. Kirschner, Phys. Rev. D **58**, 114026 (1998) [hep-ph/9807324]
8. A.D. Martin, M.G. Ryskin, T. Teubner, Phys. Rev. D **62**, 014022 (2000) [hep-ph/9912551]
9. A.V. Radyushkin, Phys. Lett. B **385**, 333 (1996) [hep-ph/9605431]; Phys. Rev. D **56**, 5524 (1997) [hep-ph/9704207]
10. D. Müller, D. Robaschik, B. Geyer, F.M. Dittes, J. Hořejši, Fortsch. Phys. **42**, 101 (1994) [hep-ph/9812448]; X. Ji, Phys. Rev. D **55**, 7114 (1997) [hep-ph/9609381]
11. J.C. Collins, L. Frankfurt, M. Strikman, Phys. Rev. D **56**, 2982 (1997) [hep-ph/9611433]
12. C. Adloff et al. [H1 Collaboration], Eur. Phys. J. C **13**, 371 (2000) [hep-ex/9902019]
13. J. Breitweg et al. [ZEUS Collaboration], Eur. Phys. J. C **6**, 603 (1999) [hep-ex/9808020]
14. J. Breitweg et al. [ZEUS Collaborations], Eur. Phys. J. C **12**, 393 (2000) [hep-ex/9908026]
15. L. Mankiewicz, G. Piller, T. Weigl, Eur. Phys. J. C **5**, 119 (1998) [hep-ph/9711227]
16. L. Mankiewicz, G. Piller, Phys. Rev. D **61**, 074013 (2000) [hep-ph/9905287]; I.V. Anikin, O.V. Teryaev, Phys. Lett. B **554**, 51 (2003) [hep-ph/0211028]
17. M. Diehl, A.V. Vinnikov, Phys. Lett. B **609**, 286 (2005) [hep-ph/0412162]
18. H.W. Huang, P. Kroll, Eur. Phys. J. C **17**, 423 (2000) [hep-ph/0005318]
19. J.B. Kogut, D.E. Soper, Phys. Rev. D **1**, 2901 (1970)
20. M. Diehl, T. Feldmann, R. Jakob, P. Kroll, Nucl. Phys. B **596**, 33 (2001) [Erratum B **605**, 647 (2001)] [hep-ph/0009255]
21. M. Diehl, Eur. Phys. J. C **19**, 485 (2001) [hep-ph/0101335]
22. M. Diehl, Phys. Rept. **388**, 41 (2003) [hep-ph/0307382]
23. J. Botts, G. Sterman, Nucl. Phys. B **325**, 62 (1989); H. Li, G. Sterman, Nucl. Phys. B **381**, 129 (1992)
24. R. Jakob, P. Kroll, Phys. Lett. B **315**, 463 (1993) [Erratum B **319**, 545 (1993)] [hep-ph/9306259]
25. P.A.M. Dirac, Rev. Mod. Phys. **21**, 392 (1949); H. Leutwyler, J. Stern, Ann. Phys. (N.Y.) **112**, 94 (1978)
26. V.L. Chernyak, A.R. Zhitnitsky, Phys. Rept. **112**, 173 (1984); P. Ball, V.M. Braun, Phys. Rev. D **54**, 2182 (1996) [hep-ph/9602323]
27. J. Bolz, J. Körner, P. Kroll, Z. Phys. A **350**, 145 (1994)
28. B. Guberina, J.H. Kühn, R.D. Peccei, R. Rückl, Nucl. Phys. B **174**, 317 (1980); S. Balk, J.G. Körner, G. Thompson, F. Hussain, Z. Phys. C **59**, 283 (1993)
29. S.J. Brodsky, G.P. Lepage, in Perturbative Quantum Chromodynamics, edited by A. Mueller (World Scientific, Singapore 1989)
30. M. Vanderhaeghen, P.A. Guichon, M. Guidal, Phys. Rev. D **60**, 094017 (1999) [hep-ph/9905372]
31. J.C. Collins, D.E. Soper, Nucl. Phys. B **193**, 381 (1981) [Erratum B **213**, 545 (1983)]; Nucl. Phys. B **194**, 445 (1982)
32. P. Kroll, M. Raulfs, Phys. Lett. B **387**, 848 (1996) [hep-ph/9605264]
33. M. Neubert, B. Stech, in Heavy Flavours II, edited by A.J. Buras, M. Lindner (World Scientific, Singapore 1997)
34. K. Schilling, G. Wolf, Nucl. Phys. B **61**, 381 (1973)
35. M. Dahm, R. Jakob, P. Kroll, Z. Phys. C **68**, 595 (1995) [hep-ph/9503418]
36. I.V. Musatov, A.V. Radyushkin, Phys. Rev. D **61**, 074027 (2000) [hep-ph/9905376]
37. M. Diehl, T. Feldmann, R. Jakob, P. Kroll, Eur. Phys. J. C **39**, 1 (2005) [hep-ph/0408173]
38. M. Diehl, T. Feldmann, R. Jakob, P. Kroll, Eur. Phys. J. C **8**, 409 (1999) [hep-ph/9811253]
39. J.W. Negele et al., Nucl. Phys. Proc. Suppl. **128**, 170 (2004) [hep-lat/0404005]
40. M.V. Polyakov, C. Weiss, Phys. Rev. D **60**, 114017 (1999) [hep-ph/9902451]
41. J. Pumplin, D.R. Stump, J. Huston, H.L. Lai, P. Nadolsky, W.K. Tung, JHEP **0207**, 012 (2002) [hep-ph/0201195]

42. A.D. Martin, R.G. Roberts, W.J. Stirling, R.S. Thorne, Phys. Lett. B **531**, 216 (2002) [hep-ph/0201127]; Eur. Phys. J. C **28**, 455 (2003) [hep-ph/0211080]
43. J. Blümlein, H. Böttcher, Nucl. Phys. B **636**, 225 (2002) [hep-ph/0203155]
44. C. Adloff et al. [H1 Collaboration], Phys. Lett. B **483**, 360 (2000) [hep-ex/0005010]
45. M. Derrick et al. [ZEUS Collaboration], Phys. Lett. B **380**, 220 (1996) [hep-ex/9604008]
46. S. Aid et al. [H1 Collaboration], Nucl. Phys. B **468**, 3 (1996) [hep-ex/9602007]
47. H1 Collaboration, contribution to the International Europhysics Conference on High Energy Physics, EPS03, Aachen (Germany) 2003
48. ZEUS Collaboration, contribution to the International Europhysics Conference on High Energy Physics, Budapest (Hungary) 2001 (Abstract 594)
49. ZEUS Collaboration, contribution to the International Conference on High Energy Physics, Beijing (China) 2004 (Abstract 6-0248)
50. K. Goeke, M.V. Polyakov, M. Vanderhaeghen, Prog. Part. Nucl. Phys. **47**, 401 (2001) [hep-ph/0106012]
51. J.B. Bronzan, G.L. Kane, U.P. Sukhatme, Phys. Lett. B **49**, 272 (1974)
52. G.K. Eichmann, J. Dronkers, Phys. Lett. B **52**, 428 (1974)
53. J. Bartels, M. Loewe, Z. Phys. C **12**, 263 (1982)
54. A.D. Martin, M.G. Ryskin, Phys. Rev. D **57**, 6692 (1998) [hep-ph/9711371]; A.G. Shuvaev, K.J. Golec-Biernat, A.D. Martin, M.G. Ryskin, Phys. Rev. D **60**, 014015 (1999) [hep-ph/9902410]
55. A.V. Belitsky, D. Müller, A. Kirchner, Nucl. Phys. B **629**, 323 (2002) [hep-ph/0112108]
56. J. Nemchik, N.N. Nikolaev, B.G. Zakharov, Phys. Lett. B **341**, 228 (1994) [hep-ph/9405355]
57. I. Royen, Phys. Lett. B **513**, 337 (2001) [hep-ph/0006044]
58. I. Ivanov, PhD thesis, hep-ph/0303053
59. A. Tripet [Spin muon Collaboration], Nucl. Phys. Proc. Suppl. **79**, 529 (1999) [hep-ex/9906008]